B. TECH. PROJECT REPORT

On

Design and Development of Shape-Memory Alloy Actuated Micro-Flapper for Aerial Robot

BY

Akash Kumar Jain
Aniket Jadhav
Gaurav Karmarkar

DISCIPLINE OF MECHANICAL ENGINEERING
INDIAN INSTITUTE OF TECHNOLOGY INDORE

December 2016

Design and Development of Shape-Memory Alloy Actuated Micro-Flapper for Aerial Robot

A PROJECT REPORT

Submitted in partial fulfillment of the requirements for the award of the degrees

of

BACHELOR OF TECHNOLOGY
In
MECHANICAL ENGINEERING

Submitted by:

Akash Kumar Jain
Aniket Jadhav
Gaurav Karmarkar

Guided by:
Dr. I.A.Palani (Assistant Professor)

INDIAN INSTITUTE OF TECHNOLOGY INDORE
December 2016

CANDIDATE'S DECLARATION

We hereby declare that the project entitled **"Design and Development of Shape-Memory Alloy Actuated Micro-Flapper for Aerial Robot"** submitted in partial fulfillment for the award of the degree of Bachelor of Technology in 'Mechanical Engineering' completed under the supervision of **Dr, I. A. Palani, Assistant Professor, Mechanical Engineering,** IIT Indore is an authentic work.

Further, we declare that we have not submitted this work for the award of any other degree elsewhere.

Signature and Name of the Student(s) with Date

–

CERTIFICATE by BTP Guide(s)

It is certified that the above statement made by the students is correct to the best of my/our knowledge.

Signature of BTP Guide(s) with Dates and their Designation

PREFACE

This report on **“Design and Development of Shape-Memory Alloy Actuated Micro-Flapper for Aerial Robot”** is prepared under the guidance of **Dr, I. A. Palani.**

Through this report, we have tried to give a detailed design of an innovative way of using an SMA Bimorph in an Ornithopter-based MAV Mechanism and we have even developed an UTM for the analysis of the mechanical properties of the bimorph. A control system for the regulation of voltage and current to the bimorph for joule heating was also fabricated. We have tried to cover every aspect of the new design, and to conclude if the design is technically and economically sound and feasible.

We have tried to the best of our abilities and knowledge to explain the content in a lucid manner. We have also added 3-D models, reference images, relevant graphs, comparative tables, photos and figures to make it more illustrative.

Akash Kumar Jain
Aniket Jadhav
Gaurav Karmarkar
B. Tech. IV Year
Discipline of Mechanical Engineering
IIT Indore

ACKNOWLEDGEMENTS

We wish to thank **Dr. I. A. Palani** for his kind support and valuable guidance.

This work has been done in framework of the IIT Indore Project that is funded by the PRIUS (Promotion of Research & Innovation for Undergraduate Student).

We would like to acknowledge Mr. Akash K., Mr. Dhiraj Narayane, Mechatronics and Instrumentation Lab, Manufacturing Processes Lab, Central Workshop and Sophisticated Instrumentation Centre of IIT Indore for providing their sincere cooperation and guidance to carry out this research.

It is their help and support, due to which we have been able to complete the design and the technical report of this project.

Without their support, this report would not have been possible.

Akash Kumar Jain
Aniket Jadhav
Gaurav Karmarkar
B.Tech. IV Year
Discipline of Mechanical Engineering
IIT Indore

ABSTRACT

In this report, we aim to use Shape Memory Alloy (SMA) Bimorph as actuators in micro-flappers for Micro-Aerial Vehicles. Shape Memory Alloy Bimorphs have some unique properties like high energy density, two-way memory effect, etc. These properties make SMA based actuators, strong contenders to replace the conventional motor –based actuators.

The SMA bimorph sheets were developed using the thermal vapor deposition method. The composition of the alloy was also varied and its effects on the phase transformation temperatures were studied. Various experiments like life-cycle analysis, load-frequency analysis, XRD test, etc. were conducted for checking the suitability of the SMA Bimorph actuator for the required purpose.

A control system was designed to provide a pulse with the desired amplitude and pulse width. A touch-less control system was also integrated later for facilitating ease in spatial control.

A Universal Testing Machine specially dedicated to studying the physical properties of Shape Memory Alloy actuators was developed. It has special features like an integrated temperature control system, tensile-compressive-cyclic loading, etc.

The design, fabrication, working, simulations, experiments and theoretical calculations will be discussed in the report.

TABLE OF CONTENTS

Chapter 3 : Experiments And Analysis

Chapter 4 : Finalized Design

Chapter 5 : Electronic Design and Interfacing

LIST OF FIGURES

LIST OF TABLES

CHAPTER 1 : INTRODUCTION

1.1 What is a Micro-Aerial Vehicle (MAV)?

The term micro air vehicle (MAV) refers to a new type of remotely controlled unmanned aerial vehicle (UAV) that is significantly smaller than similar aircrafts, obtainable by using state-of-the-art technology. The target dimension for MAVs today is approximately 15 centimeters (six inches) and development of insect-sized aircrafts is reportedly expected in the near future. Potential military use is one of the driving factors, although MAVs are also being used commercially and in scientific, police, and mapping applications.

Micro Air Vehicle (MAV) has the capability to fly autonomously in complex environments which enables human to conduct surveillance in areas which are deemed too dangerous or in confined spaces that do not allow human entry. Research and development of MAVs aim to reduce their size further. Thus, novel techniques need to be explored in order to achieve this objective while still maintaining the MAVs' current performance.

Controlling the flights of Aerial Vehicle is a difficult task and is not something which could be accomplished by an amateur. Also, till date, almost all the control systems for AVs use remote controllers, which do not allow for control over more than 3 degrees of freedom (DOF). As AVs can have up to 6 DOF, especially the sophisticated ones, it is high time to have an easy to use system.

MAVs may be broadly classified into two types – Multicopters and Ornithopters. Currently, both multicopters and ornithopters are using motor-based mechanisms to satisfy their flight requirements, which have a lot of room for improvement.

a) Multicopters

Multicopters basically use a set of vertically oriented propellers to generate lift required for flight. It is a simple aerial vehicle whose motion is controlled by controlling multiple downward thrusting propeller units.

Quadcopters are one of the most common type of multicopter MAVs. A quadcopter can control its roll and pitch rotation by speeding up two motors on one side and slowing down the other two. So, if it wanted to roll left it would speed up motors on the right side of the frame and slow down the two on the left. If it wants to rotate forward it speeds up the back two motors and slows down the front two. Figure 1 below shows an illustrative model of a quadcopter; a type of multicopter.

Figure 1 : Illustration of a Multicopter

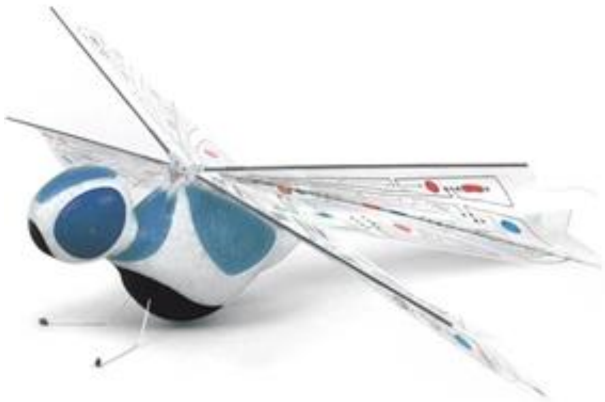

Figure 2 : Illustration of an Ornithopter

b) Ornithopters

Ornithopters represent the category of aircrafts which use a flapping mechanism for flight, instead of using propellers. The physical structure and flying mechanism of the ornithopters are both increasingly inspired by insects or birds found in nature.

Flapping wings work on the same principle as an airplane propeller, except they are moving back and forth. The wings flap with an up-and-down motion, usually. But as they do so, they also move forward through the air along with the rest of the bird. Close to the body, there is very little up and down movement. Farther out toward the wingtips, there is much more vertical motion. Figure 2 included above displays an illustrative model of an Ornithopter-based MAV.

1.2 Drawbacks of the Current Designs of MAV

The current MAVs, though quite interesting, do have their drawbacks.

- They have complex control systems,
- High power battery and motors greatly increases the total weight of the system.
- Most of them using rotors, make a lot of noise, making stealth operations quite difficult.
- Components, if damaged, are not very easy to replace.
- Manufacturing them is an expensive business.

1.3 What is Shape Memory Alloy (SMA)?

Shape memory alloys (SMAs) are metals that "remember" their original shapes. SMAs are useful for such things as actuators which are materials that "change shape, stiffness, position, natural frequency, and other mechanical characteristics in response to temperature or electromagnetic fields". The potential uses for SMAs especially as actuators have broadened the spectrum of many scientific fields. The study of the history and development of SMAs can provide an insight into a material involved in cutting-edge technology. The diverse applications for these materials have made them increasingly important and visible to the world.

SMAs have two stable phases: the high-temperature phase, called austenite and the low-temperature phase, called martensite. The martensite can be in one of two forms: twinned or detwinned. A phase transformation which occurs between these two phases upon heating/cooling is the basis for the unique properties of the SMAs.

Upon cooling in the absence of applied load the material transforms from austenite into twinned martensite (no observable macroscopic shape change occurs). Upon heating the material in the martensitic phase, a reverse phase transformation takes place and as a result the material transforms to austenite.

If mechanical load is applied to the material in the state of twinned martensite (at low temperature), it is possible to it. Even upon releasing the load, the material remains deformed.

A subsequent heating of the material to a temperature above the austenite finish temperature (A_f - temperature at which transformation of martensite to austenite is complete) will result in a reverse phase transformation (martensite to austenite) which will lead to a complete shape recovery of the SMA.

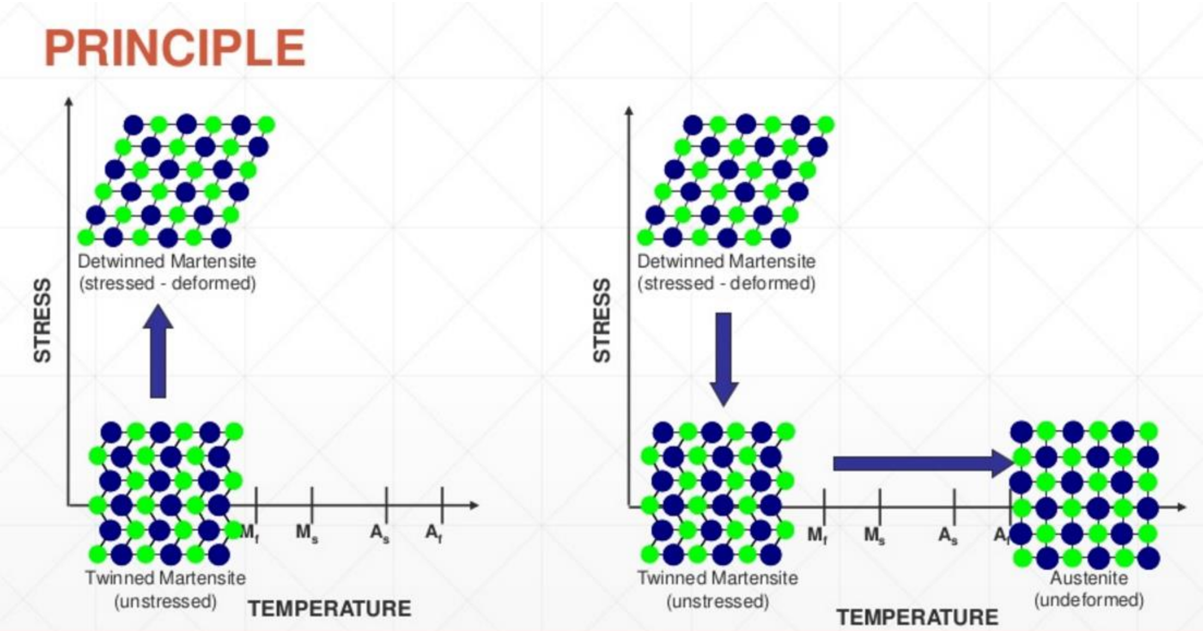

Figure 1 : Phase Transformations in SMA

The schematic shown above in Figure 3 demonstrate the phase transformation principle involved in the development of shape memory effect in SMA. It shows a variation of stress with temperature. The first graph shows the conversion of twinned martensite to detwinned martensite as a result of development of thermal stresses while the second graph shows the complete austenite to martensite conversion cycle in case of SMA.

SMA remembers the shape when it has austenitic structure. So, if we need SMA to remember and regain/recover certain shape, the shape should be formed when structure is austenite. Reheating the material will result in complete shape recovery.

Shape-memory materials behave differently. They're strong, lightweight alloys with a very special property. They can be "programmed" to remember their original shape, so if you bend or squeeze them you can get that original shape back again just by heating them. This is called the ‘Shape-Memory Effect’.

1.4 Shape Memory Effect

Shape-memory alloys have different types of shape-memory effects. Two common effects are one-way shape memory effect and two-way shape memory effect. The procedures are very similar for both: starting from martensite (a), adding a reversible deformation for the one-way effect or a severe deformation with an irreversible amount for the two-way (b), heating the sample (c)and cooling it again (d).

a) One-Way Shape Memory Effect

When a shape-memory alloy is in its cold state (below A_s), the metal can be bent or stretched and will hold those shapes until heated above the transition temperature. Upon heating, the shape changes to its original. When the metal cools again it will remain in the hot shape, until deformed again. With the one-way effect, cooling from high temperatures does not cause a macroscopic shape change. A deformation is necessary to create the low-temperature shape. On heating, transformation starts at A_s and is completed at A_f. Figure 4 below demonstrates the One Way Shape Memory Effect (OWSME).

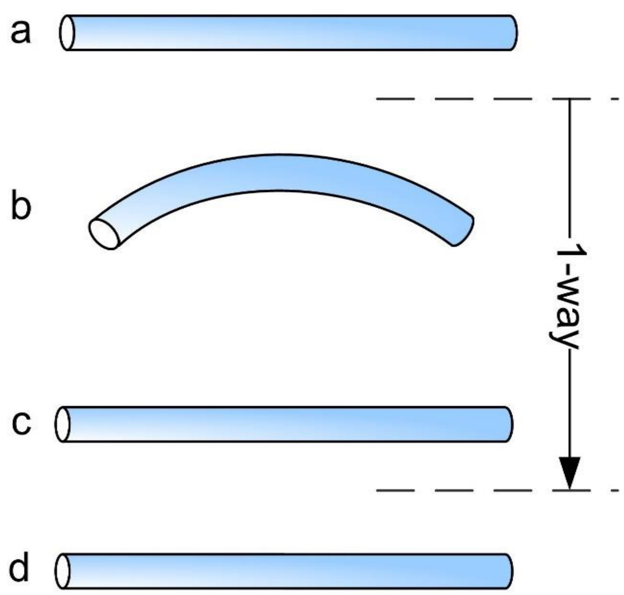

Figure 4 : One Way Shape Memory Effect (OWSME)

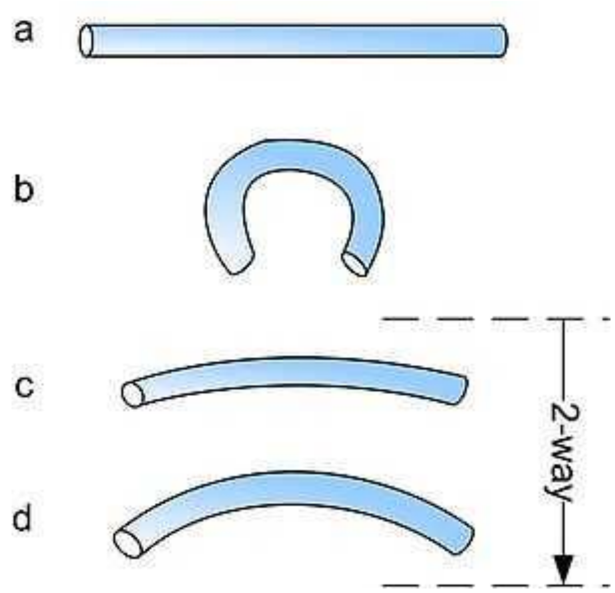

Figure 5 : Two Way Shape Memory Effect (TWSME)

b) Two-Way Shape Memory Effect

The two-way shape-memory effect is the effect that the material remembers two different shapes: one at low temperatures, and one at the high-temperature shape. Such a material shows a shape-memory effect during both heating and cooling. This can also be obtained without the application of an external force (intrinsic two-way effect). The reason the material behaves so differently in these situations lies in training. Training implies that a shape memory can "learn" to behave in a certain way. Under normal circumstances, a shape-memory alloy (SMA) "remembers" its low-temperature shape, but upon heating to recover the high-temperature shape, immediately "forgets" the low-temperature shape. However, it can be "trained" to "remember" to leave some reminders of the deformed low-temperature condition in the high-temperature phases. There are several ways of doing this. A shaped, trained object heated beyond a certain point will lose the two-way memory effect. The Figure 5 above demonstrates the Two Way Shape Memory Effect (TWSME).

1.5 Motivation behind the Project

Autonomous micro-helicopters will soon play a major role in tasks like search and rescue, environment monitoring, security surveillance, and inspection. If they are further realized in small scale, they can also be used in narrow outdoor and indoor environments and represent only a limited risk for people.

Most of the micro-aerial vehicles that are currently in the development stage have motor actuated wings to provide the necessary thrust it requires to hover. We have identified that Shape-Memory Alloys (SMAs) could be used instead of the motor-actuated wings to produce the flapping motion in the micro-flapper. The two-way memory effect of the SMA bimorph sheet could be exploited to serve as an actuator for the flapping wing mechanism in ornithopters.

Also, SMAs have a high energy density which too can be harnessed for our benefit. The shortcomings of the current MAV mechanisms, the potential which SMAs have in this field and the prospect of combining them together contributed to the motivation behind this project.

CHAPTER 2 : CONCEPT DESIGN

2.1 Implementation of SMA Actuators in Micro-Aerial Vehicles

The functionality of modern Micro-Aerial-Vehicles(MAVs) can be significantly enhanced by reducing their weight and size. For the past two decades, engineers have been working on overcoming these constraints by optimizing the various parameters involved like design, material selection, flight mechanism etc. The concept of Nano-Aerial-Vehicles has also become popular in recent times.

While other parameters have evolved significantly over the years, the flight mechanism (flapping wing) has not seen many changes. Motors which were traditionally being used as wing actuators are being used even today in MAVs. This constrains the scope of applications of MAVs due to the restrictions imposed on size and weight by the flight mechanism.

An alternative flight mechanism should have some essential features like-

- Small size and low weight
- High energy density
- Ability to provide high frequencies of actuation
- Quick response for better flight control

Shape Memory Alloy(SMA) actuators exhibit all the mentioned essential features and thus can be a viable option for replacing the motors used in the flight mechanisms of traditional Micro-Aerial Ornithopters.

The advantages of using SMA actuators are -

- Available in all shapes and sizes (Can be easily tailored to suit the requirement).
- Actuation properties (like Actuation Temperature) can be easily controlled by varying the composition of the SMA.
- Flight control requires a very basic control system and a low power on-board supply.
- Large work output per unit of actuator mass.
- Rapid thermal cycling due to large surface area to volume ratio.
- Super elasticity.

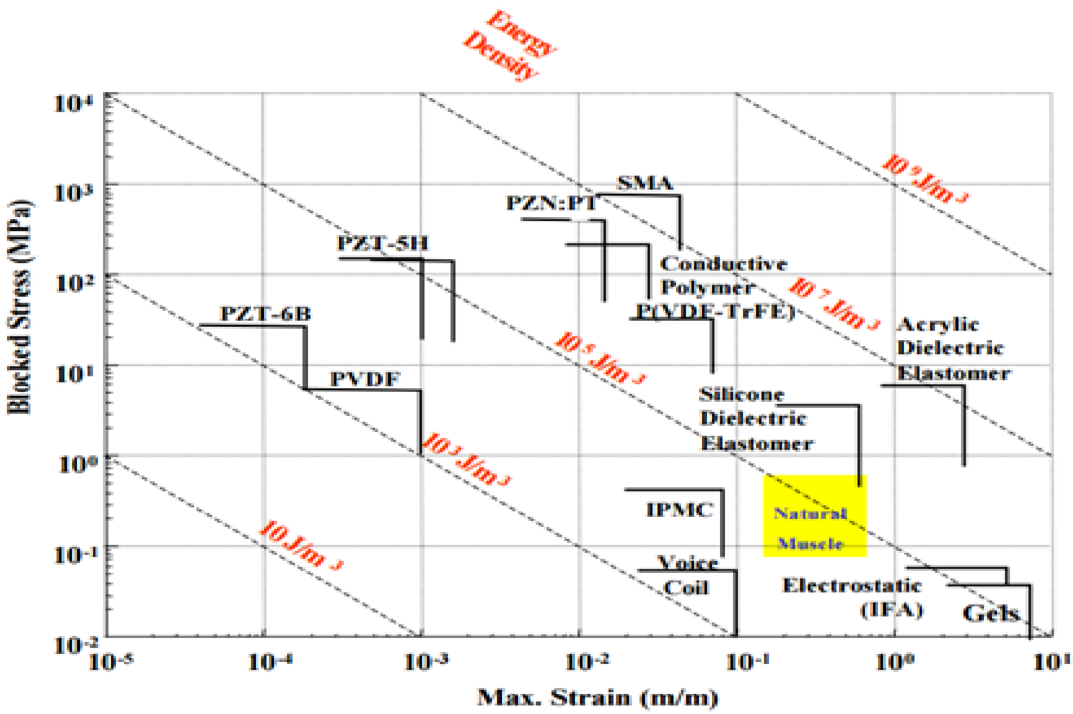

Figure 6 : Energy Density Comparison

There are 3 major types of Shape Memory Alloy actuators -

1. Shape Memory Alloy Bimorphs
2. Shape Memory Alloy Wires
3. Shape Memory Alloy Springs

The flight mechanism of Micro-Aerial Ornithopters requires reciprocating motion which is difficult to achieve using SMA wires or springs, given the size constraints. Also, SMA springs and SMA wires, in most cases, only show One Way Shape Memory Effect, which cannot give the required reciprocating motion. Hence SMA Bimorphs are most suitable to be used as actuators for the flight mechanism.

The advantages of using SMA Bimorph Actuators over SMA Springs/Wires are -

- SMA Bimorphs exhibit the 'Two-way Memory Effect'. The two-way shape-memory effect is the effect owing to which the material remembers two different shapes: one at low temperatures, and another one at the high-temperature shape. A material that shows a shape-memory effect during both heating and cooling is said to exhibit a two-way shape memory. This can also be obtained without the application of an external force (intrinsic two-way effect).

- Unlike SMA Springs/Wires, SMA Bimorphs need not be trained to remember the shapes. Due to the difference in physical properties of the polyimide substrate (Kapton Sheet) and the shape memory alloy, some thermal stresses are developed during its deposition. When at higher temperatures, the phase of the SMA changes, these thermal stresses are overcome by the shape memory effect and there is a change in shape. When the temperature is decreased again, the thermal stresses bring it back to its original shape.
- While using Joule heating, SMA Bimorphs can be actuated at a lower voltage than SMA Springs/Wires. They also require comparatively lesser time for cooling due the availability of a larger surface area.

The most common Shape Memory Alloys used as SMA Bimorph actuators are -

- Ni-Ti based alloys
- Cu-Al-Ni based alloys
- Cu-Zn based alloys

Considering the requirement of robustness in the flight mechanism, Cu-Al-Ni based SMAs are ideal for this application. The phase transformation temperature for Cu-Al-Ni (81.5% by weight of Cu, 14% by weight of Al and 4.5% by weight of Ni) is around 220-230°C and thus the actuation of the SMA is not much affected by changes in ambient temperatures. This also ensures that there are no significant discrepancies in flight control even in extreme environments.

2.2 Conceptual Design for Incorporation of Shape Memory Alloy Bimorph Actuator as Micro-Flapper in Micro-Aerial Vehicles

Two strips of the SMA Bimorph will be mounted on each side of the chassis of the Micro-Aerial-Vehicle. The wings (made of X) will be attached as an extension of the SMA Bimorph. The power supply and control system will be mounted on the chassis.

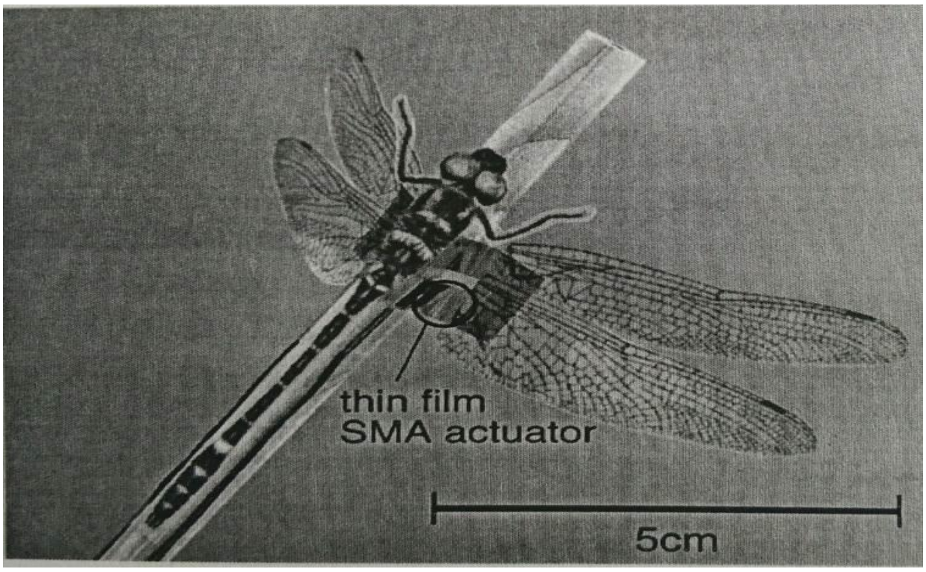

Figure 7 : Conceptual Design of MAV

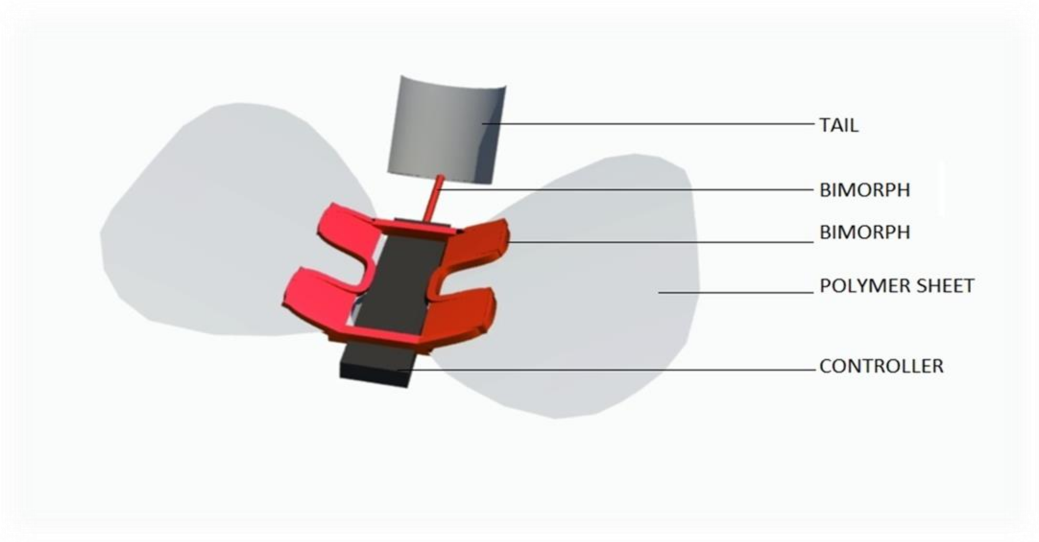

Figure 8 : 3D Model of Conceptual Design

Figure 7 included above shows the conceptual design as planned for this MAV and its 3D model and Figure 8 shows its 3D model.

2.3 Conceptual Design for Universal Testing Machine

Physical properties play a vital role in determining the scope of applications of Shape Memory Alloys. It is also important to study the variations of these physical properties in Shape Memory Alloys with variations in temperature and phase changes. Thus, to cater to these needs, a Universal Testing Machine with high precision, special clamping system and temperature control was designed and fabricated.

Figure 9 included below shoes a 3D model of this UTM. The maximum load to be applied on conventional SMA actuators is very low. Hence, a load cell of low load capacity but high precision was selected.

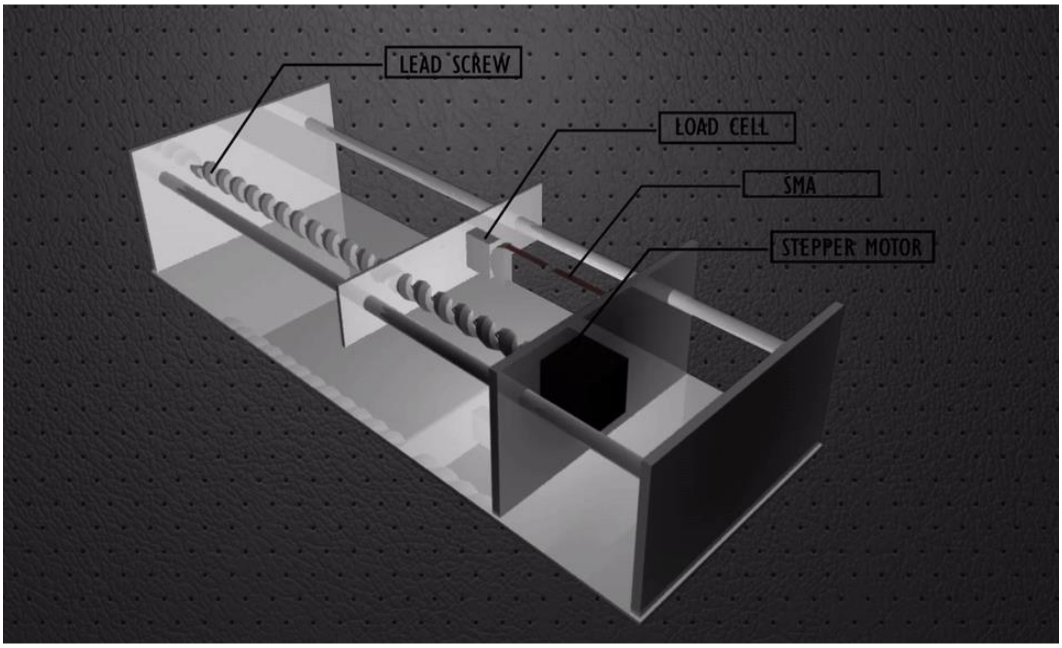

Figure 9 : 3D model of UTM

The clamps for SMA wires, springs and bimorphs were separately designed because of the variations in their shapes and sizes. The clamps were designed in a way, such that the load distribution throughout the SMA actuator specimen, was be uniform.

A provision for the inclusion of water bath was provided for testing the physical properties at different temperatures.

Additional features like an easy-to-use interface, variety of loading patterns and clamps etc. are also provided.

CHAPTER 3 : EXPERIMENTS AND ANALYSIS

3.1 Development of SMA Bimorph

This project involved the use of SMA for MAV's micro-flapper. As discussed previously, three options were available to choose from – SMA spring, SMA wire and SMA bimorph. And as the bimorph had an advantage of having two-way actuation; which the spring and wire did not have; SMA bimorphs were preferred over spring or wire.

But unlike SMA springs and wires, SMA bimorphs are not commercially available. Also, since the optimal composition and other properties necessary for our parameters were not known, it was necessary to develop them in-house.

Now, a lot of different processes are available which can be used to develop thin films, but vacuum deposition methods are the most prominent ones. These operate at pressures well below atmospheric pressure (i.e., vacuum). The deposited layers can range from a thickness of one atom up to millimeters, forming freestanding structures. The process can be qualified based on the vapor source; physical vapor deposition uses a liquid or solid source and chemical vapor deposition uses a chemical vapor.

Any deposition process requires a substrate to be used as a base on which the deposition is to be done. Kapton has the ability to maintain its excellent physical, electrical, and mechanical properties over a wide temperature range. A flame-resistant material, Kapton polyimide retains good strength above 500°C for a short time, and has a zero-strength temperature above 800°C. There is no known organic solvent for the film and it is infusible and does not melt. Adhesives are available for bonding Kapton polyimide to itself, to metals, and to other films.

Using the available PVD setup, which utilized the evaporation deposition process, SMA bimorph sheets using kapton polyimide as substrate for deposition for Cu-Al-Ni were developed.

a) Physical Vapor Deposition

Physical Vapor Deposition (PVD) is a collective set of processes used to deposit thin layers of material, typically in the range of few nanometers to several micrometers. PVD processes are environmentally friendly vacuum deposition techniques consisting of three fundamental steps:

- Vaporization of the material from a solid source assisted by high temperature vacuum or gaseous plasma.
- Transportation of the vapor in vacuum or partial vacuum to the substrate surface.
- Condensation onto the substrate to generate thin films.

Different PVD technologies utilize the same three fundamental steps but differ in the methods used to generate and deposit material. Some of the different methods which are included in Physical Vapor Deposition are: Cathodic Arc Deposition, Electron Beam Physical Vapor Deposition, Evaporative Deposition, Pulsed Laser Deposition, Sputter Deposition, Sublimation Sandwich Method etc. The two most common PVD processes are thermal evaporation and sputtering.

Deposited films can span a range of chemical compositions based on the source material(s). Further compositions are accessible through reactive deposition processes. Relevant examples include co-deposition from multiple sources, reaction during the transportation stage by introducing a reactive gas (nitrogen, oxygen or simple hydrocarbon containing the desired reactant), and post-deposition modification through thermal or mechanical processing.

From among the methods mentioned above, evaporation deposition process was used owing to the availability of the related setup and apparatus.

b) Evaporation Deposition

Evaporation is one of the most common methods of thin-film deposition. The source material is evaporated in a vacuum. The vacuum allows vapor particles to travel directly to the target object (substrate in our case), where they condense back to a solid state. The schematic shown in Figure 10 below displays the setup used for the evaporation PVD process, briefly mentioning all the components including tungsten boat, power supply and substrate.

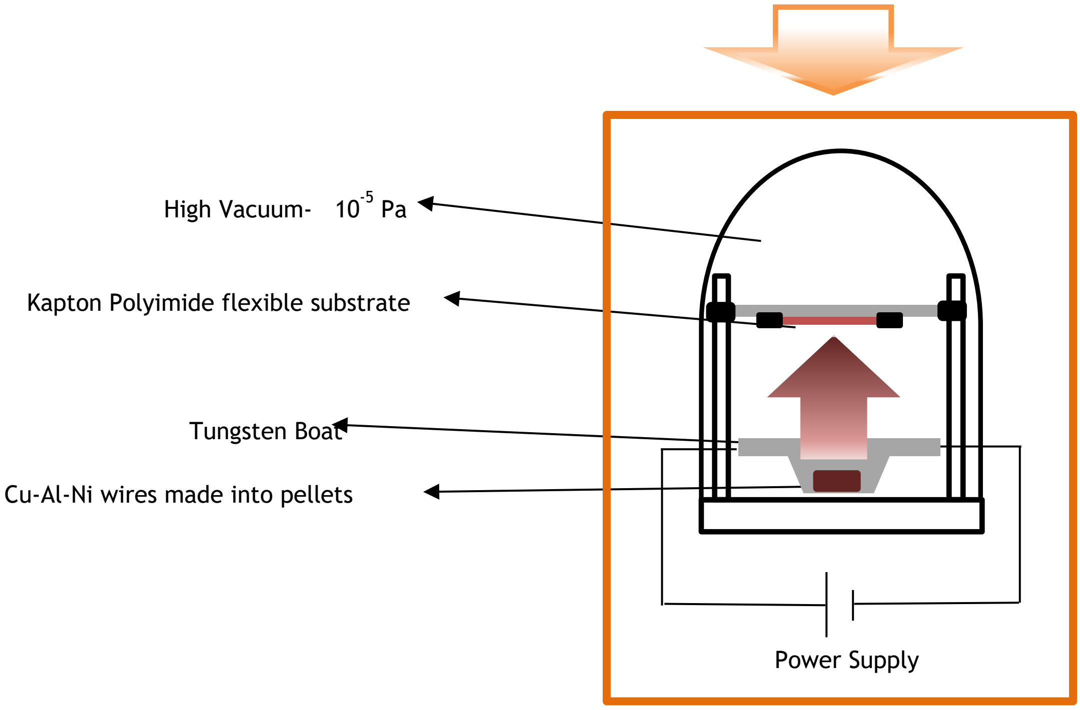

Figure 10 : Thin Film Deposition on Kapton Polyimide Flexible Substrate using PVD

Evaporation takes place in a vacuum, i.e. vapors other than the source material are almost entirely removed before the process begins. In high vacuum, evaporated particles can travel directly to the deposition target without colliding with the background gas. The tungsten boat contains the individual elements used for the coating process (Cu, Al and Ni in our case), which are then gradually heated to melting point temperature of the element which has the highest melting point. After all the elements have melted, the temperature is again gradually raised to boiling point temperature of the element which has the highest boiling point.

At this point, the temperature is increased further, causing the mixture of elements thus formed to evaporate and then deposit on the substrate which is placed right above the tungsten boat. This complete procedure leads to the formation of the kapton-based SMA bimorph.

During this process, care must be taken to ensure that a proper vacuum has been formed. Else the presence of oxygen in air inside the chamber, if a proper is not formed, may lead to the formation of oxides with metals, ruining the SMA bimorph.

3.2 XRD Analysis of Bimorph Sheet

Since the sheets were developed in-house, there was a very high probability of not getting the proper composition. Even a slight variation in composition disturbs the properties of the bimorph. It may lead to noticeable variations in the properties like actuation temperature, crystalline structure, brittleness etc. So, confirmation of deposition composition was mandatory. For this, XRD technique was used.

X-ray diffraction (XRD) is an analysis technique primarily used for phase identification of a crystalline material and can provide information on unit cell dimensions, crystalline structure or average bulk composition. The actual setup used is shown below in Figure 11.

XRD works basically on the principle of Bragg's Diffraction formula:

$$\lambda = 2d_{hkl} \sin(\theta)$$

Figure 11 : Actual XRD Setup

For parallel planes of atoms, with a space 'd_{hkl}' between the planes, constructive interference only occurs when Bragg's law is satisfied. When this happens, a peak for intensity is observed for the corresponding value of 'θ' as in Bragg's Law. In our diffractometers, the X-ray wavelength 'λ' is fixed. Consequently, a family of planes produces a diffraction peak only at a specific angle 'θ'. Additionally, the plane normal must be parallel to the diffraction vector. The space between diffracting planes of atoms determines peak positions. The peak intensity is determined by what atoms are in the diffracting plane.

From the literature available, the value of ‘θ’ corresponding to the composition used in the bimorphs for this project is found to be approximately 45°.

Figure 12 and Figure 13 included below show the variation of the intensity with the angle ‘θ’ obtained for two of the specimens of the Bimorphs:

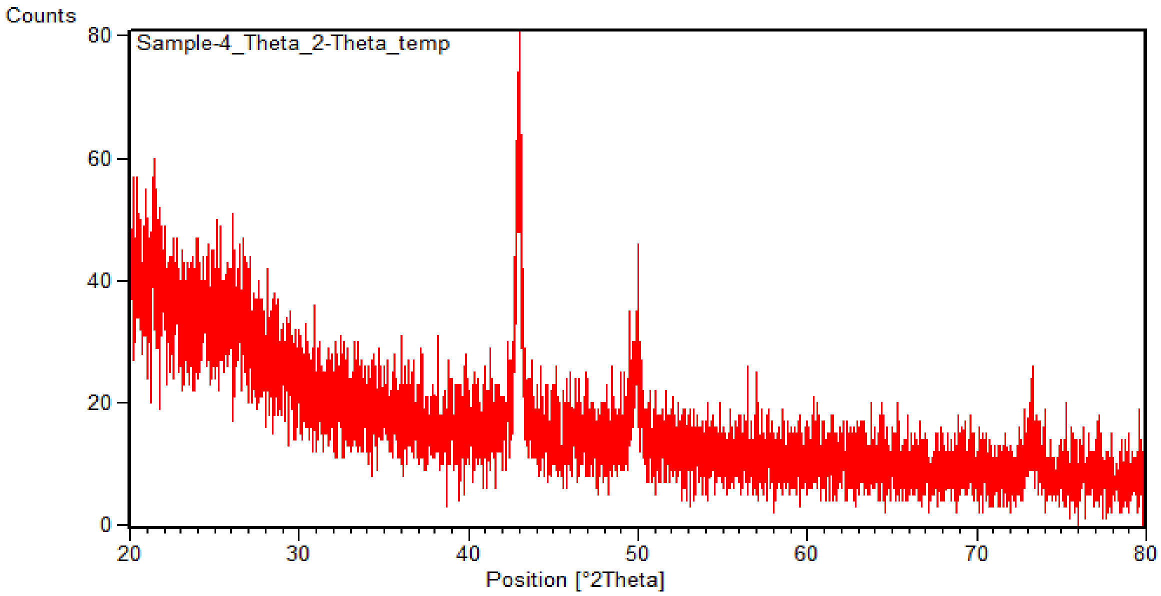

Figure 12 : XRD Analysis Result 1

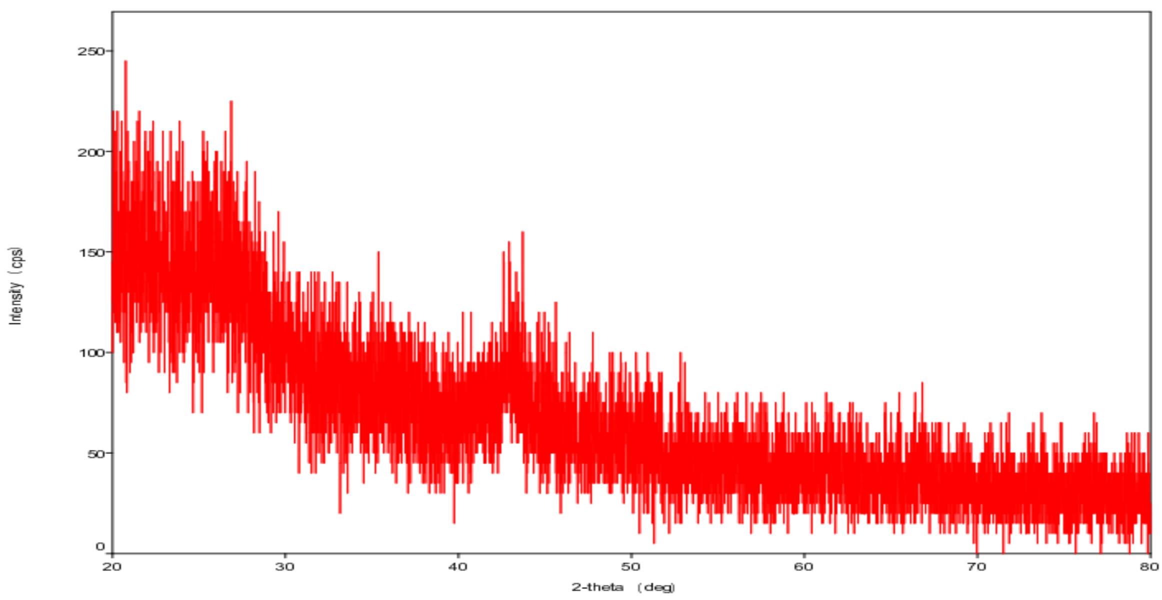

Figure 13 : XRD Analysis Result 2

In both the above results, it could be seen that a peak for the intensity is observed at approximately 45°, indicating that the composition deposited is what was intended.

3.3 Analysis of Bimorph using Profilometer

During the process of deposition, there is a possibility that the substrate used may not be smooth; or that the deposition did not take place evenly. There might be the presence of cracks within the deposition. Evaporated atoms that collide with foreign particles may react with them; or may also reduce the amount of vapor that reaches the substrate, which makes the thickness difficult to control.

Evaporated materials deposit non-uniformly if the substrate has a rough surface. Because the evaporated material attacks the substrate mostly from a single direction, protruding features block the evaporated material from some areas. This phenomenon is called "shadowing" or "step coverage."

If the deposition in not uniform, if there is too much roughness on the surface or if there is presence of cracks; then there is a possibility of burning of the sheet during joule heating, right along these cracks or other region having lower deposition thickness.

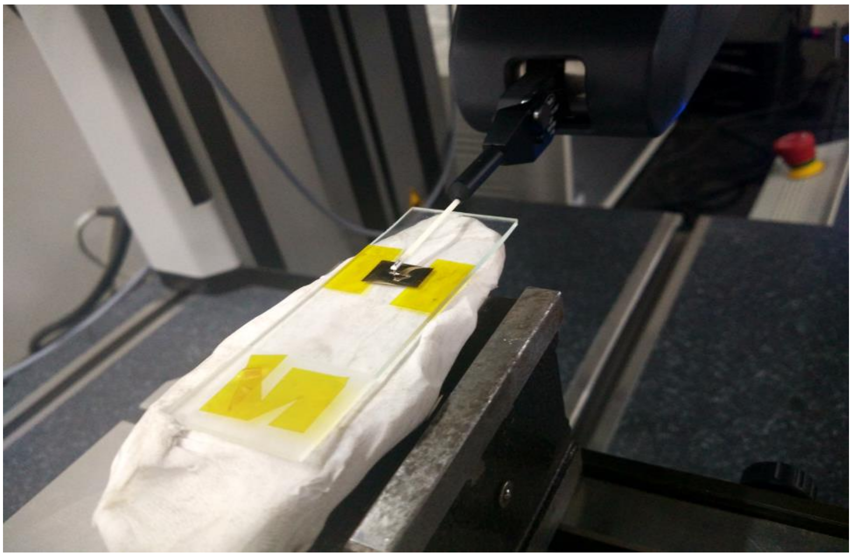

Figure 14 : Actual Profilometer Setup

The actual profilometer experimental setup used for this task is shown above in Figure 14. To check the uniformity of deposition, a profilometer was used after making a groove in the bimorph; which went all the way down to the substrate. It provided the roughness profile displaying the texture of the deposition surface and the depth of the groove observed in the roughness profile revealed the thickness of deposition.

a) Surface Roughness Analysis

Figure 15 below shows a 3-diensional view of the surface roughness profile for the entire surface of the said bimorph:

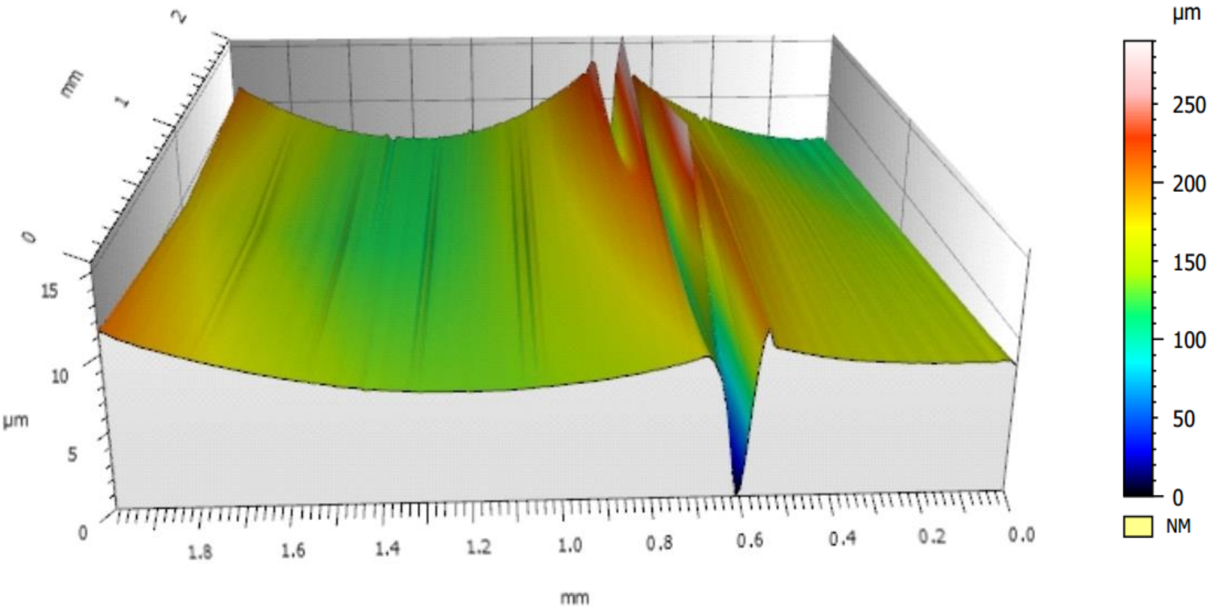

Figure 15 : 3D view of Roughness Profile

For the above result, the X-axis displays the distance from one end of the bimorph sheet and the Y-axis displays the height from the top surface of the substrate. The height at different points can be inferred from the above graph., thus giving a proper estimate of the roughness profile for the bimorph.

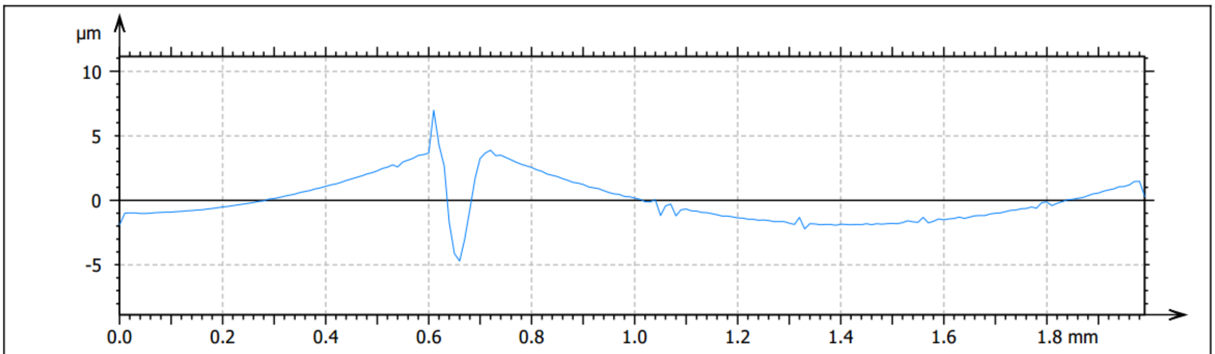

Parameters	Value	Unit
Length	1.99	mm

Figure 16 : Roughness Profile Result

Figure 16 is a front view of Figure 15, showing same details with the exact same parameters on both the axes, providing an estimate of the thickness through the depth of the groove.

b) Measurement of Deposition Thickness

The above Figure 16 is the actual graph of the surface profile without the application of the Gaussian Filter. But as can be seen; the profile is too curvy, which may not necessarily be the actual case. The curve may be a result of improper placement of the bimorph or some other factor. This unusual behavior may lead to wrong conclusions about the thickness of the deposition layer.

So, in order to compensate for this, the Gaussian Filter is applied. Gaussian filter smoothens the curve to the limit defined but cut-off wavelength; to get the non-groove part of it to zero. This flattens the unconcerned portion of the graph and adjusts the remaining part in accordance to it to give a more accurate estimation of the deposition thickness.

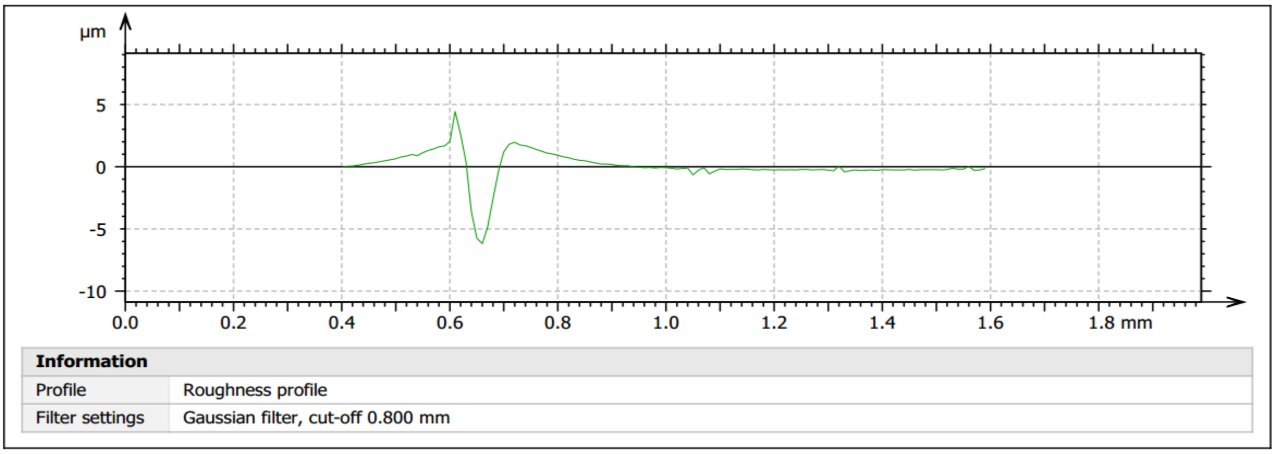

Figure 17 : Roughness Profile Result after applying Gaussian Filter

Figure 17 above shows the previous Figure 16 with the application of Gaussian Filter. In this, the curviness has been compensated for using a cut-off wavelength of 0.8 mm for the Gaussian Filter. It also has the same axes parameters as those in Figure 16, and the depth of the groove in this one gives a more accurate value for the thickness of the deposition layer on the bimorph, as opposed to that in Figure 16.

3.4 Life Cycle Analysis of Developed Bimorph Sheets

The bimorph sheets developed are supposed to be used as micro-flappers for MAV. So, they are supposed to be robust. Also, they should be able to sustain the actuation properties for a long period of time or at least for the time period of one mission which it is supposed to be used for.

Joule heating would be the preferred method of actuation in order to maintain the compactness and portability of the MAV. But this involves a probability of failure of the bimorph after prolonged usage; since joule heating would apply continuous thermal stresses on it, which may lead to fatigue failure.

So, in order to ensure that the bimorph withstands the required usage, it was put through a series of tests for life cycle analysis.

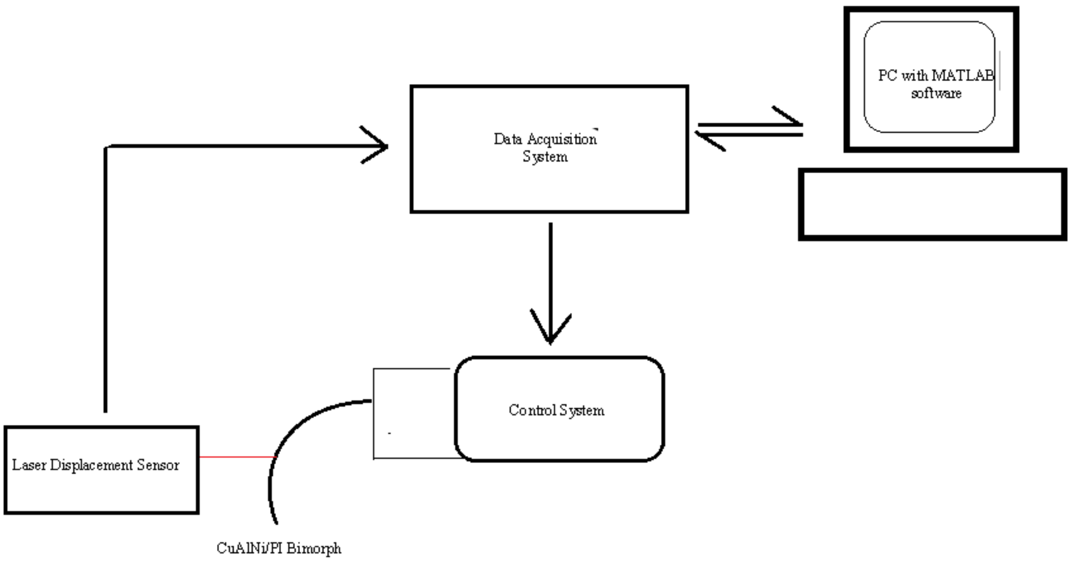

Figure 18 : Circuit Diagram for Life-Cycle Analysis Setup

The Figure 18 included above shows a schematic of the life-cycle analysis setup used. It consisted of a Laser Displacement Sensor (LDS) for measuring the displacement of the bimorph, a DAQ system for recording the values of displacement and a Programmable Power Supply (PPS) for providing the alternating voltage at the required frequency. A PC was connected to this setup in which the observed values were recorded. Crocodile clips were used in the initial stages to establish the contact and ensure the flow of current.

Figure 19 below shows the bimorph part of the actual setup used:

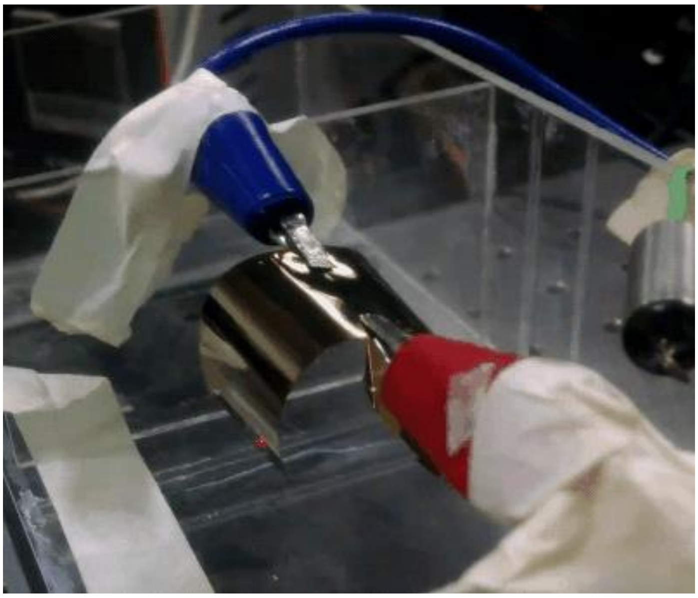

Figure 19 : Actual Setup for Life-Cycle Analysis

The analysis was done for a number of samples. All the bimorphs were tested for a duration of 1000 cycles; each having equal heating and cooling time. The recorded values for the displacement of the bimorph were plotted as a function of time.

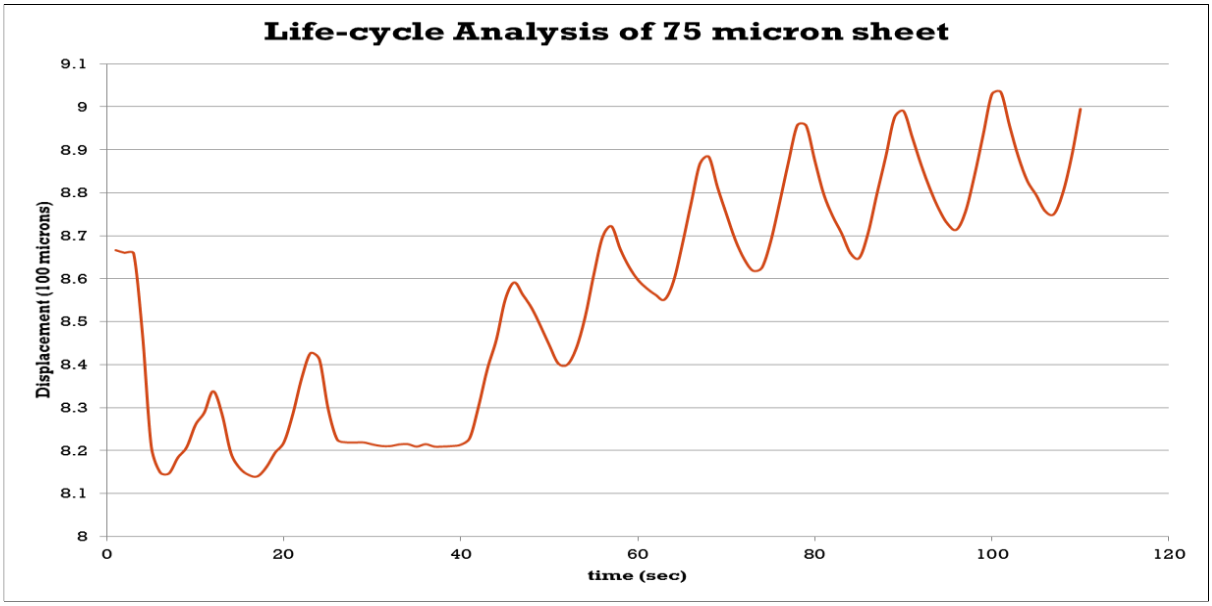

Figure 20 : Life-Cycle Analysis Graph for a 75 Micron Sheet

Figure 20 above shows a smaller part of the graph of displacement plotted as a function of time for a bimorph having a kapton substrate of 75 micron thickness.

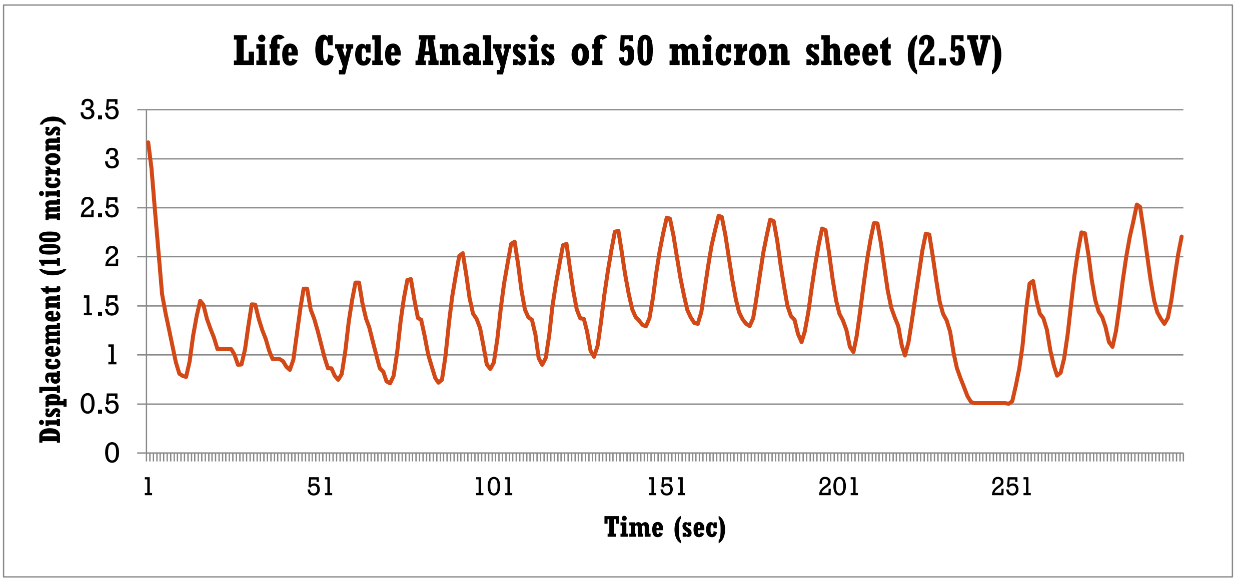

Figure 21 : Life-Cycle Analysis Graph for a 50 Micron Sheet

Figure 21 above shows a smaller part of a similar graph of displacement plotted as a function of time; this time for a bimorph having a kapton substrate of 50 micron thickness.

In both the cases, a voltage of 2.5 V was passed and the observations were taken for different cycle times ranging from a single to second to about 10 seconds. The value of current observed varied as per the change in voltage and so did the power generated.

After multiple repetitions of the above analysis for different bimorphs, it was observed that the shape memory effect prevails even after 1000 cycles and no change even in the magnitude of displacement take place. This is true in case of most of the bimorphs.

Some bimorphs did happen to fail. Some of the primary reasons for this failure may be described as under:

- When an attempt was made to increase the voltage in order to get a higher displacement, bimorph got overheated which lead to burning.
- The use of crocodile clips for contacts lead to the development of high contact resistance, producing more power and thus burning the sheet. Also, crocodile clips lead to physical damage of the bimorph at the point of contact.
- Some bimorphs, which had an uneven surface profile and the presence of cracks, as expected, burnt along those irregular surfaces, thus leading to fatigue failure.

3.5 Frequency Measurements for Developed Bimorph Sheets

After the completion of the life-cycle analysis, it was concluded that there is no fatigue failure in the bimorph and the shape memory effect was still observable even after a repetition of 1000 cycles.

But as can be seen in figures 20 and 21 showing the graphs for the life-cycle analysis, the displacement observed was too small. Also, the PPS used for the above setup was not consistent enough with the alternation of the supply of voltage, which is evident from the irregularities and the discontinuations visible in the graph.

So, the control system shown in figure 37 in the latter part of this report was used since it provided the required square waves with better regularity. Also, the bimorphs of Cu-Al-Ni used previously were modified with the addition of a small quantity of Mn, as literature suggests that addition of Mn leads to lowering of actuation temperature; which would in-turn translate to a lower power requirement.

So, the same setup as that of the life-cycle analysis was used; with the only difference being that of an improved bimorph and the substitution of PPS by the self-designed control system. Further, the voltage was increased for 2.5 V to 5 V, with the expectation of achieving a higher displacement at a higher frequency.

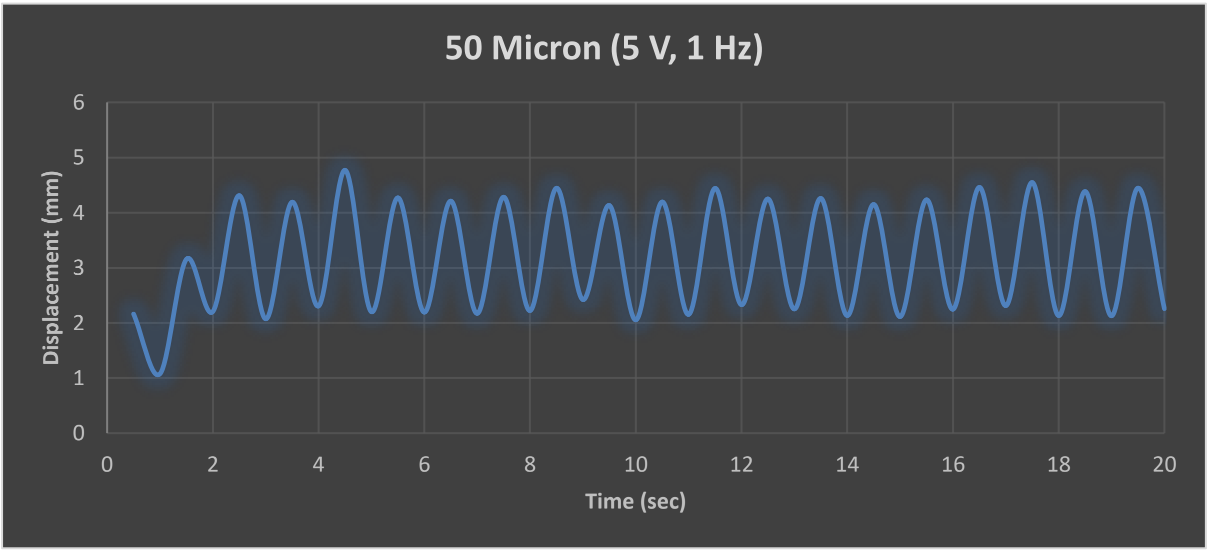

Figure 22 : Displacement as function of time at a frequency of 1 Hz

Figure 22 shown above is a graph of the displacement as a function of time at a frequency of 1 Hz; which is visible for a period of 20 seconds.

Figure 23 below shows the same plot at a frequency of 2 Hz.

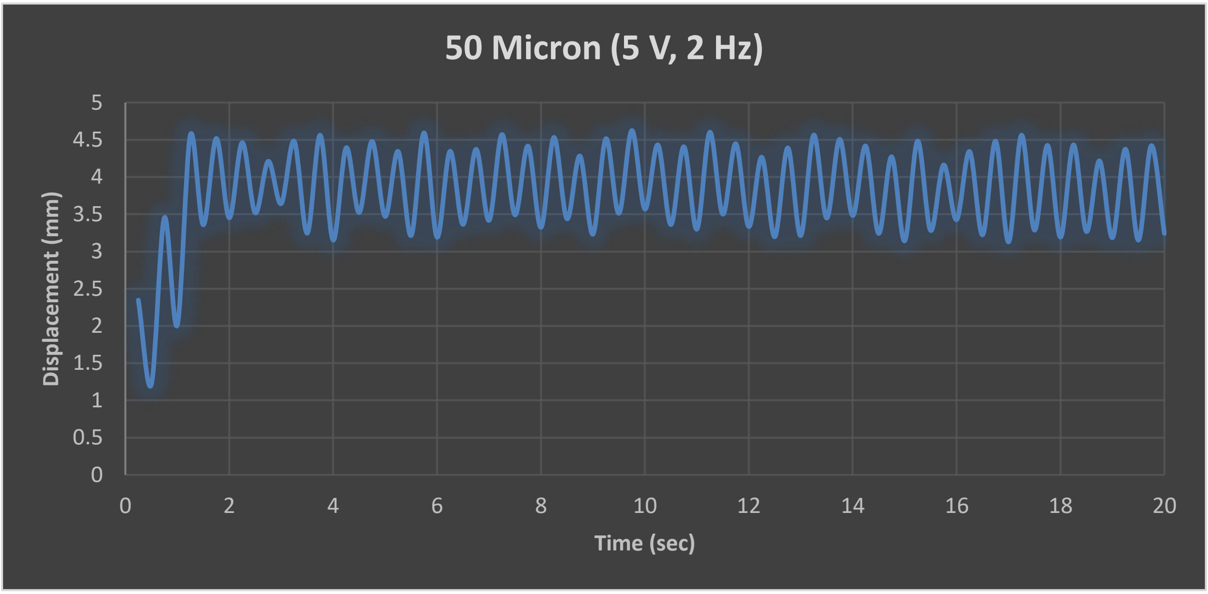

Figure 23 : Displacement as a function of time at a frequency of 2 Hz

An attempt was made to increase the frequency further, and the figure 24 below shows a plot of displacement as a function of time at a frequency of 5 Hz; again for 20 seconds.

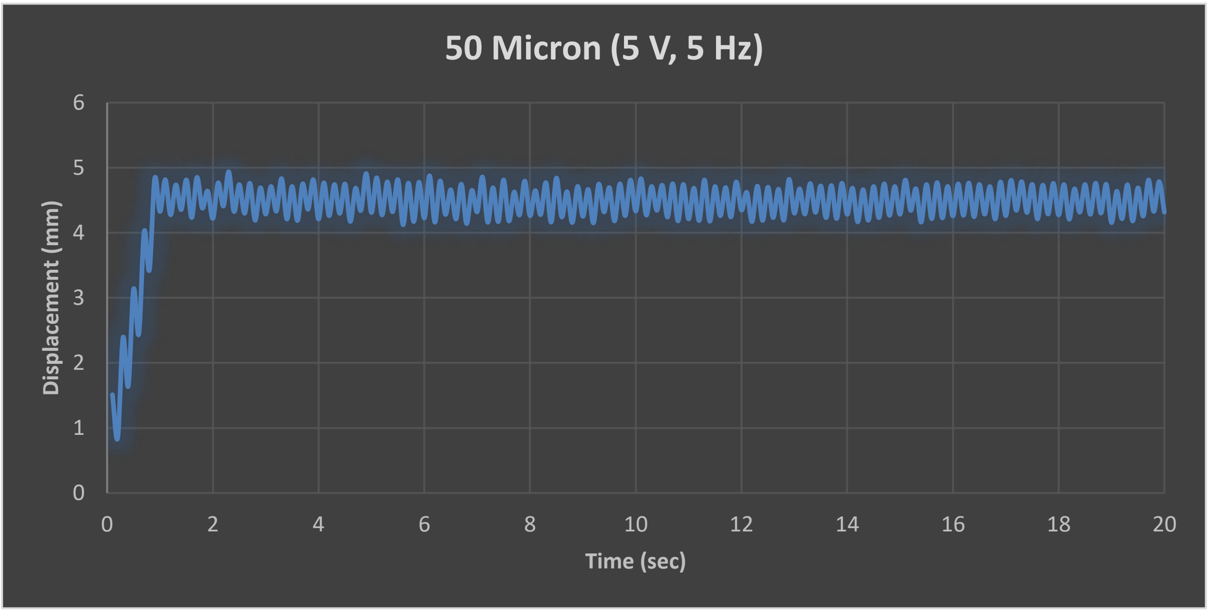

Figure 24 : Displacement as a function of time at a frequency of 5 Hz.

It was observed that as the frequency goes on increasing, the displacement goes on decreasing. After the frequency was increased beyond 5 Hz, the LDS was still able to detect the displacement; but it was no longer visible to the naked eye.

3.6 Displacement Variations for Different Loads

As the bimorphs are expected to find application in MAV, they are supposed to help it take flight. For this, they will have to generate thrust which should have the capacity to lift the entire weight of the system.

The thrust thus generated will be proportional to the area. For same material and thickness, the area will be proportional to the weight of the wing. So, the maximum limit of the area of the wing will be bound by the load capacity of the bimorph.

$$\text{Force } \alpha \text{ (Wing area) } \alpha \text{ (Weight of wing)}$$

This invokes the requirement for analyzing the capacity of the bimorph to lift the load. So, using the same setup as used in life cycle analysis and frequency investigation, the bimorph was again made to actuate; but this time with certain amount of load attached to its tip. This made the bimorph behave like a cantilever; and the force measurements could be carried out.

From one of the research papers in this regard titled "Ti– Ni– Cu shape-memory alloy thin film formed on polyimide substrate" by A. Ishida and M. Sato, a formula for calculating this force is given as,

$$F = \left(\frac{3 \times E_s \times I_s}{L^3}\right) = \left(\frac{E_s \times b \times t_s^3 \times d}{4 \times L^3}\right) = \left(\frac{E_s \times b \times t_s^3}{4 \times L}\right) \times d = K \times d$$

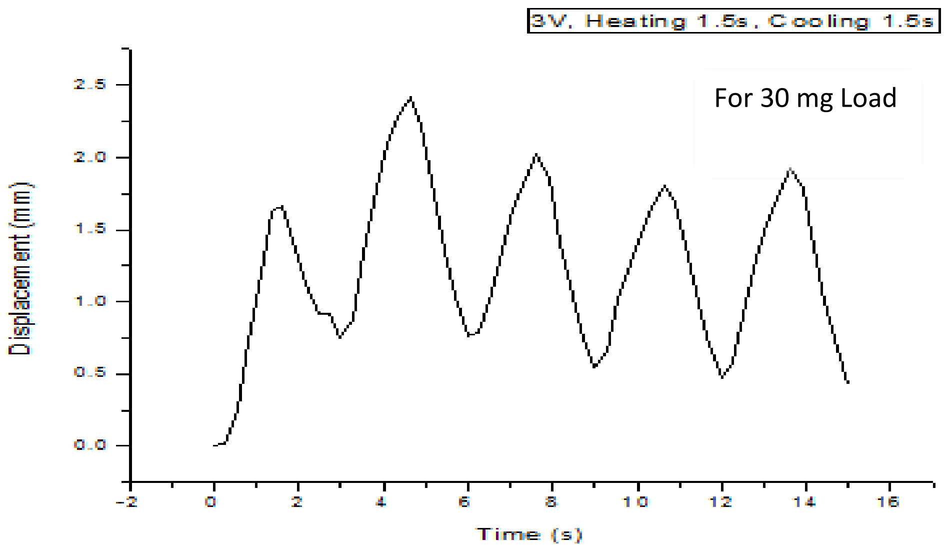

Figure 25 : Displacement-Time Graph with 30 mg Load

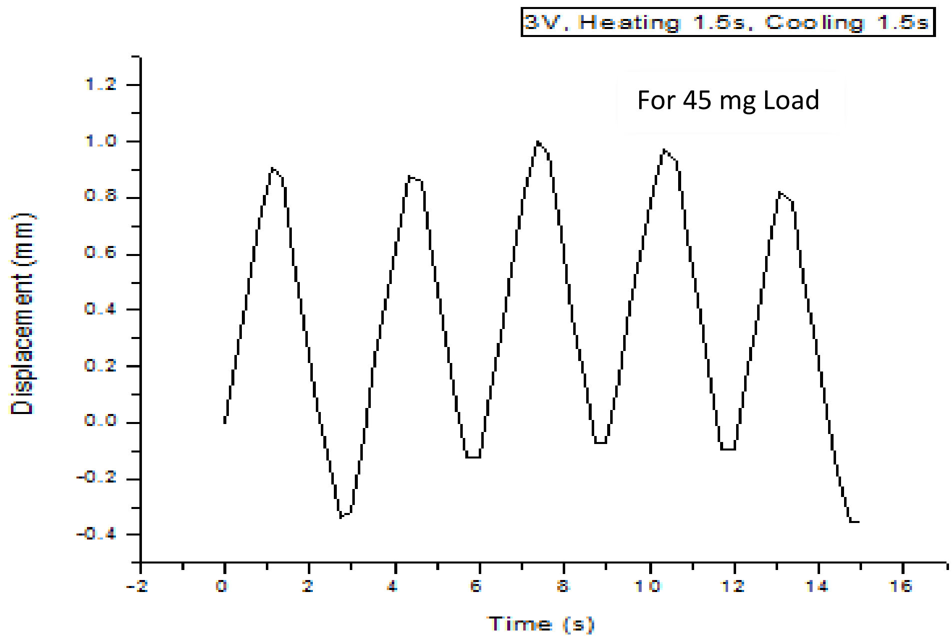

Figure 26 : Displacement-Time Graph with 45 mg Load

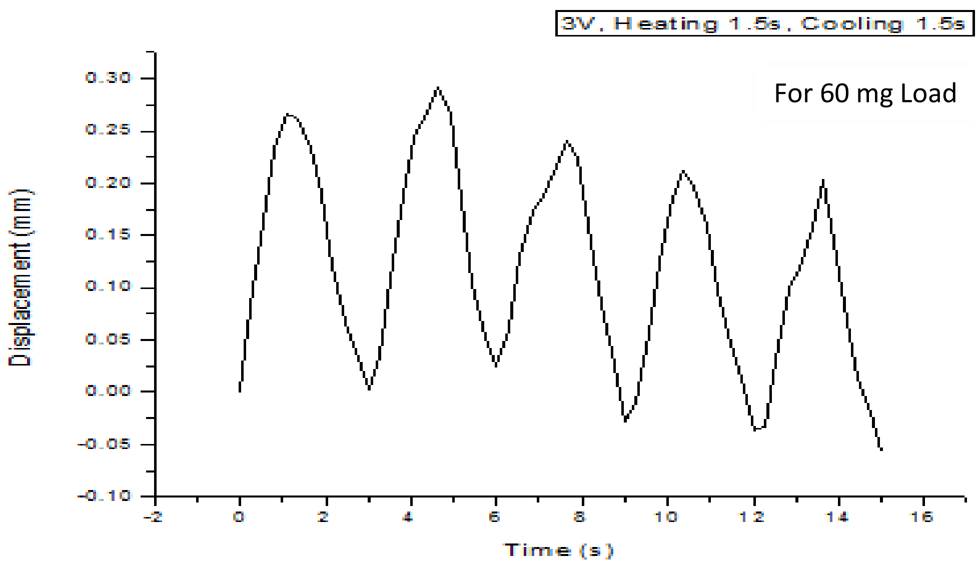

Figure 27 : Displacement-Time Graph with 60 mg Load

The figures 25, 26 and 27 above show the variation of displacement with load for different values of load as mentioned. It was observed that as the load on the bimorph was increased, the observed displacement decreased. Further analysis performed using a lot of different loads confirmed this trend.

CHAPTER 4 : FINALIZED DESIGN

4.1 Optimization of Setup Design

The experimental setup used was as shown in Figure 28. The polyimide sheet was clamped between two surfaces and was mounted on a board. It was observed that the sheet which was rectangular in shape, showed very low displacement. Even after varying the compositions of the bimorph, no significant improvement in displacement was observed.

Figure 28 : Mounted Setup for Analysis

After proper analysis, the rectangular shape of the bimorph was found to be the culprit for this low displacement. So, a change of shape of the bimorph used was mandatory. It was decided to use a U-shaped bimorph instead of a rectangular one.

The fundamental principle behind the shape change resulting in the wing-flapping mechanism is the heating-cooling cycle which was achieved through Joule heating. So, even though the current passing through the sheet was sufficient enough to actuate it, the displacement was very low because the current passed only through a small portion of the SMA bimorph sheet. To rectify this, the current had to be forced to pass through a larger area of the SMA bimorph sheet.

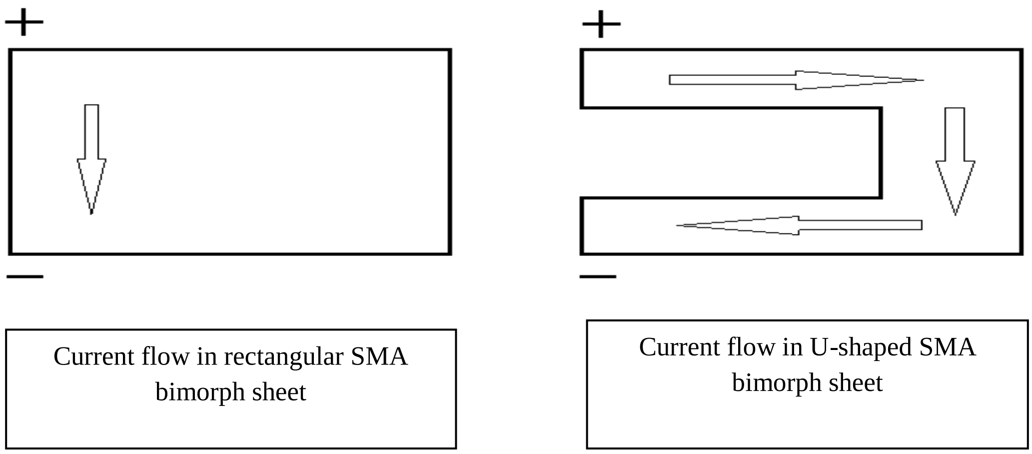

Figure 29 : Comparison of Current Flow in Rectangular and U-shaped Bimorph

This was achieved by cutting the SMA bimorph sheet in a ‘U-Shape’ as shown in Figure 29 above, which also shows the schematic of the passage of current.

A 3D model for the chassis of the Micro-Aerial Vehicle was made using Solid Works. The dimensions were decided based on the constrains imposed by the weight and size of the model and the capacity of the 3D printer to print intricate objects. The designs were optimized based on the problems encountered.

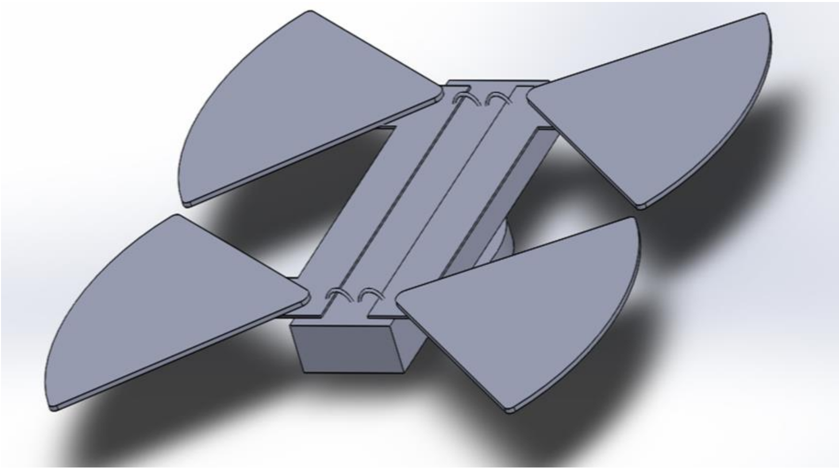

Figure 30 : Four-Wing Design for MAV

Figure 30 above shows the initial four-wing concept design. However, the implementation of this design would have required proper co-ordination between both pairs of wings, which would have been a difficult task at such an initial stage of this implementation.

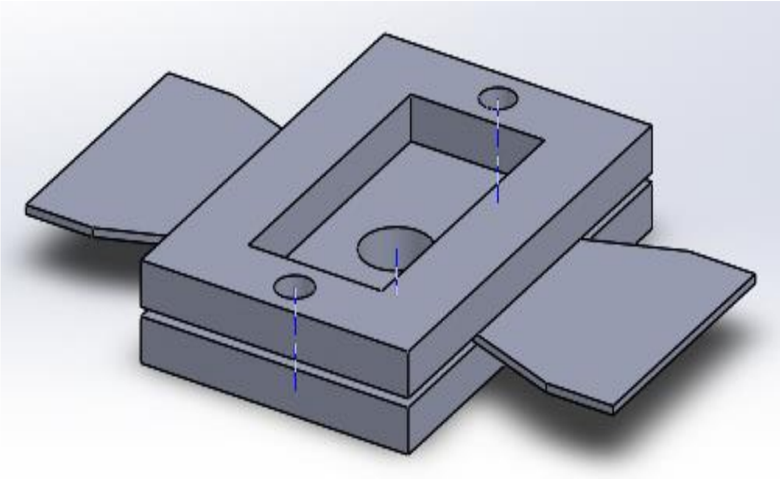

Figure 31 : Preliminary Model of MAV

Figure 31 above shows the preliminary design of MAV. However, this mechanism had complications in clamping mechanism. Also, it didn't have enough room for movement of the bimorph on actuation.

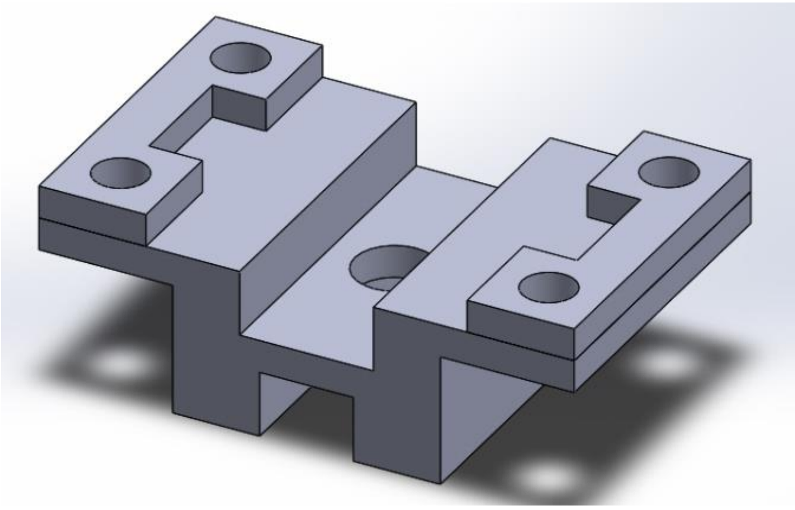

Figure 32 : Optimized Design of MAV

Figure 32 above shows the final optimized design, which had the required changes implemented. Room was provided below the extruded clamping sites for the proper movement of wings and even the clamps were reduced in size in order to avoid any loose or improper clamping of the bimorph.

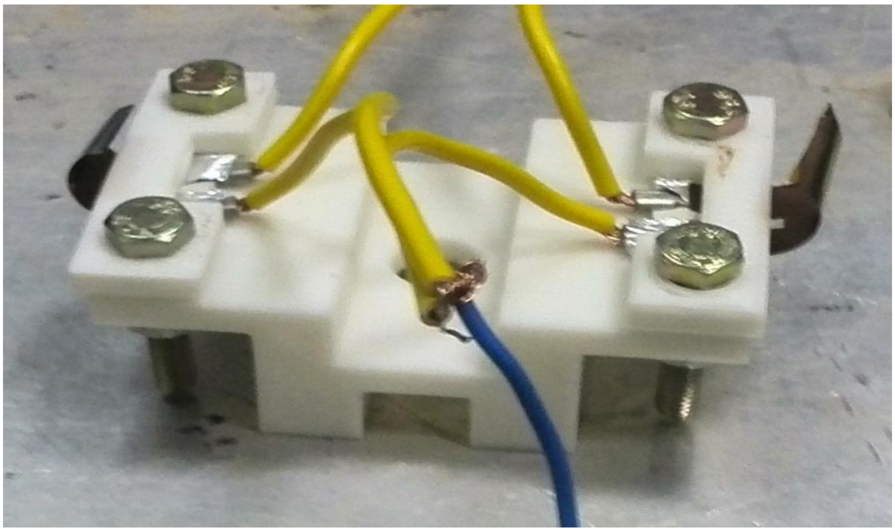

Figure 33 : Actual 3D printed model of MAV

Figure 33 above shows the final 3D printed version of the model shown in figure 32. It also shows the testing specimen of bimorph clamped in the setup.

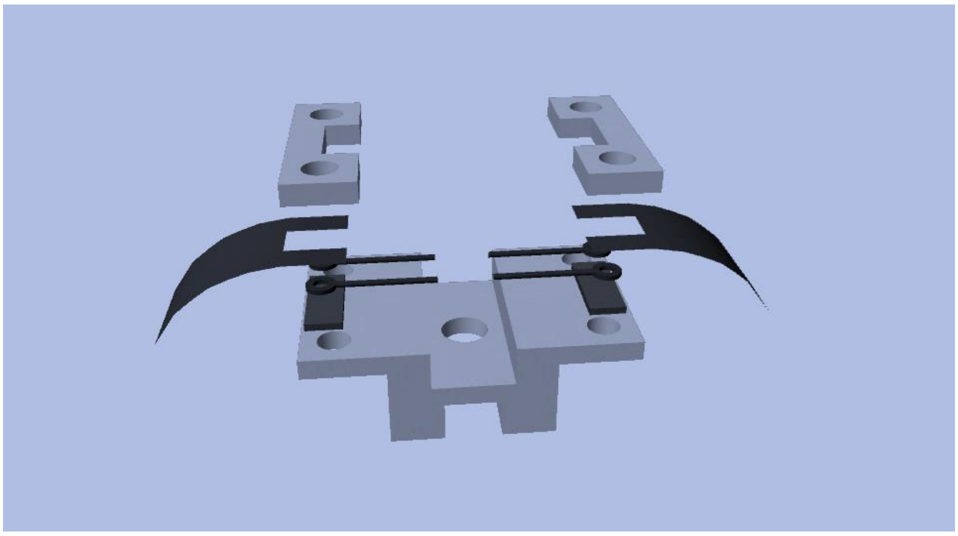

Figure 34 : Wing Position Exploded View

Figure 34 shows the exploded view of the optimized setup; which gives a proper idea of the type of clamping mechanism used. Aluminium foils were used while clamping in order to avoid any incidences of loose contact.

4.2 Force Calculations

The force produced due to the actuation in the sheet is given by -

$$F = \left(\frac{3 \times E_s \times I_s}{L^3}\right) = \left(\frac{E_s \times b \times t_s{}^3 \times d}{4 \times L^3}\right) = \left(\frac{E_s \times b \times t_s{}^3}{4 \times L^3}\right) \times d = K \times d$$

Let $\left(\frac{E_s \times b \times t_s{}^3}{4 \times L^3}\right)$ = k be some constant.

Therefore, F = k × d,

where E_s = Young's Modulus of Elasticity for the given sheet,

I_s = Its Second Moment of Inertia,

d = Displacement of the Free Edge,

t_s = Thickness of the Substrate,

b = Width of the Cantilever,

and L = Length of the Cantilever.

For the Cu-Al-Ni sheets, we have,

$E_s = 2.5$ GPa

The Dimensions of Bimorph Sheet used for this experiment were,

$t_s = 75$ microns b = 2 cm L = 2.5 cm

Also, to calculate the maximum value of 'F', the maximum attained value of 'd' through experimental procedures must be used.

This gives d = 4.5 mm

Using these values in the above formula, we get,

$F = 1.518 \times 10^{-3}$ N

Also, F = mg. Considering $g = 9.81\ m/s^2$, we get,

m = 154.74 mg

This 'm' represents the mass of system which could be lifted.

4.3 Universal Testing Machine

The salient features of the Universal Testing Machine are -

- Use of high precision load cell.
- Use of stepper motor and low-pitch lead screw for smooth application of load.
- Specially designed clamps for clamping of SMA bimorph sheets, SMA wires and SMA springs.
- Specially designed clamps to ensure uniform force distribution throughout the specimen.
- Provision of water bath for specimen temperature control.
- Easy-to-use software with features like tensile, compressive and cyclic loading.

Table 1 : Specifications of Working model of UTM

UTM Specifications		
1	Load Cell Capacity	Maximum Load 50 N (5 kg)
2	Maximum Displacement	35 cm
3	Temperature Range of Water Bath	10°C to 80°C
4	Type of Jaws for Clamping	Bimorph (Sheet)
		Wire
		Spring

The Table 1 above gives the specifications of the UTM. A load capacity of 50 N is more than enough for the limits of a bimorph sheet. Also, three different types of jaws have been developed for clamping each of bimorph, wire and spring.

Figure 35 below shows the actual developed UTM based on the final designed model. All the circuitry including the Arduino, power supply and the motor driver has been enclosed in the base of the UTM.

a) Calculations for Deformation

Change in length of Bimorph Sheet = Displacement of movable plate

Also, Displacement = Velocity × Time

Thus, displacement = $\left(\frac{\text{RPM} \times \text{Pitch} \times \text{Time}}{60}\right)$

Using this value of displacement, the strain can be calculated by using the value of displacement as an input via the developed software.

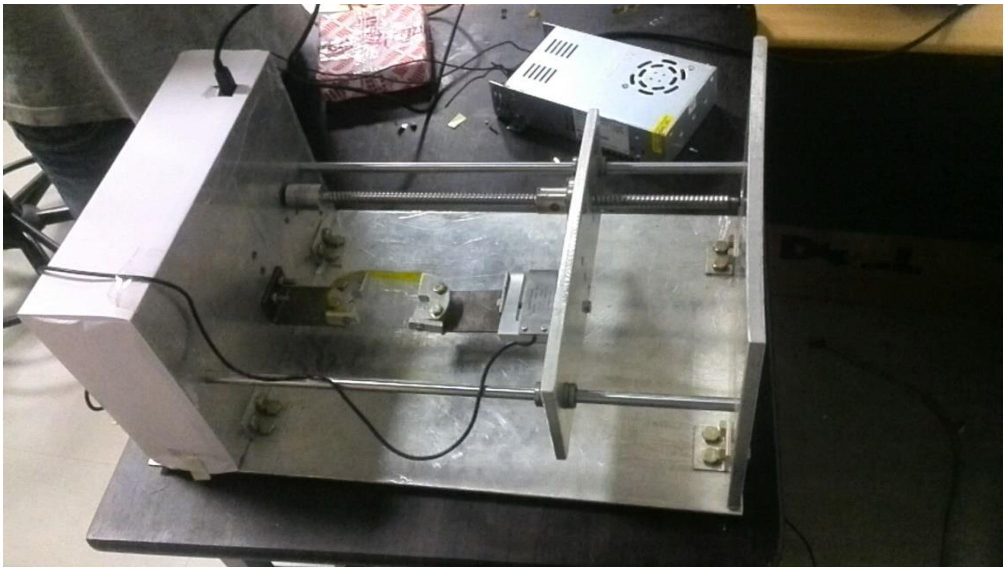

Figure 35 : Final Setup of UTM

b) Calculations for Force

Tension in Bimorph = Force across load cell

Force α Voltage across Wheatstone bridge

F = G ×V (where 'G' is the constant of proportionality)

The value of 'F' thus obtained can be used for the calculation of stress as it can be measured using load cell.

4.4 Design of the Control System

In the initial stages of the project, the 3-channel programmable power supply was used to provide the square wave for the actuation of the SMA bimorph. The programmable power supply uses a relay switch for providing a periodic pulse. Some inconsistencies were observed in the pulse wave when the displacement of the SMA bimorph sheet was measured using a Laser Displacement Sensor (LDS) for a large number of cycles during the life-cycle analysis. Also, the programmable power supply was not able to provide a pulse with frequency higher than 2 Hz. Moreover, a portable control system had to be made for use in the final prototype.

The control system has been designed to provide input voltage from 0 - 12 V. Thus, it can easily be used for actuation of other SMA actuators apart from SMA bimorph (SMA springs/wires).

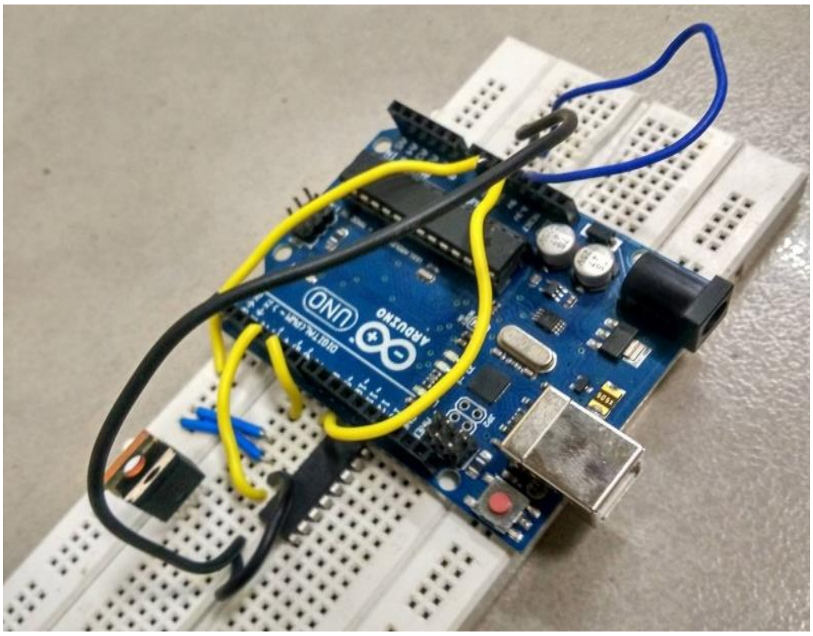

Figure 36 : Off-board Control System

An off-board control system was first designed on a bread-board using an Arduino, a MOSFET and an amplifier (L293D). The same has been shown in Figure 36 included above.

An on-board control system was also developed later on a Printed Circuit Board (PCB) with an ATmega 328p chip, a MOSFET and an Amplifier.

The control system was then integrated with a gesture-controlled system that uses the principle of capacitive touch to sense the position of the controller in 3D (a human hand in this case) in a specified zone. This gesture control can be easily used to control the flight of Micro-Aerial Vehicles.

Table 2 : Control System Parameters

Sr. No.	Parameter	Value
1	Output Voltage (Amplitude)	0-12 V
2	Output Frequency	Up to 20 Hz
3	Wave Form	Square Wave

The Table 2 above gives an idea of some of the important parameters which influence the functioning of the control system.

CHAPTER 5 : ELECTRONIC DESIGN AND INTERFACING

5.1 Control System

An Arduino-based controlled system to provide square waves of desired pulse-width and amplitude was designed. By varying the pulse-width, the heating and cooling time of bimorph can be controlled. Amplitude of the wave represents voltage value of output.

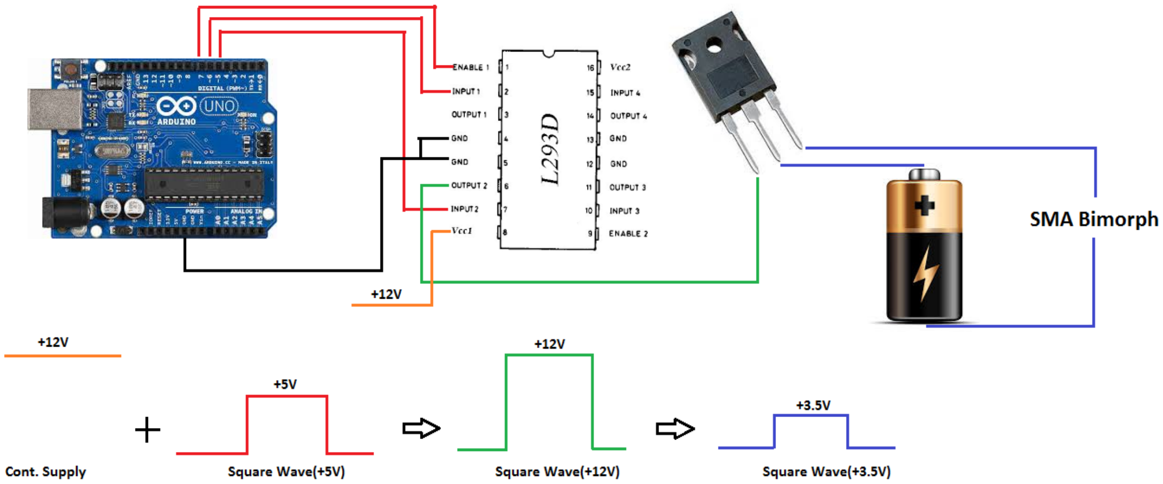

Figure 37 : Circuit Diagram of Control System

In the system shown above in Figure 37, Arduino provides voltage in the form of a square wave of amplitude 5 V to the L293D amplifier which amplifies the signal to 12V with an external 12 V input. This 12 V square wave output of L293D is transferred to a MOSFET. The MOSFET acts as a switch and completes the circuit between the first and the second pin, only when there is 12 V input to its third pin. When square wave is in its positive half, MOSFET is on; otherwise it is off. Unlike the mechanical switching used in a DC power supply, MOSFET works as an electric switch which makes it more efficient; even when operated at higher frequencies.

Figure 38 shown below is a flowchart which shows the same information as mentioned above, depicting the course of actions followed.

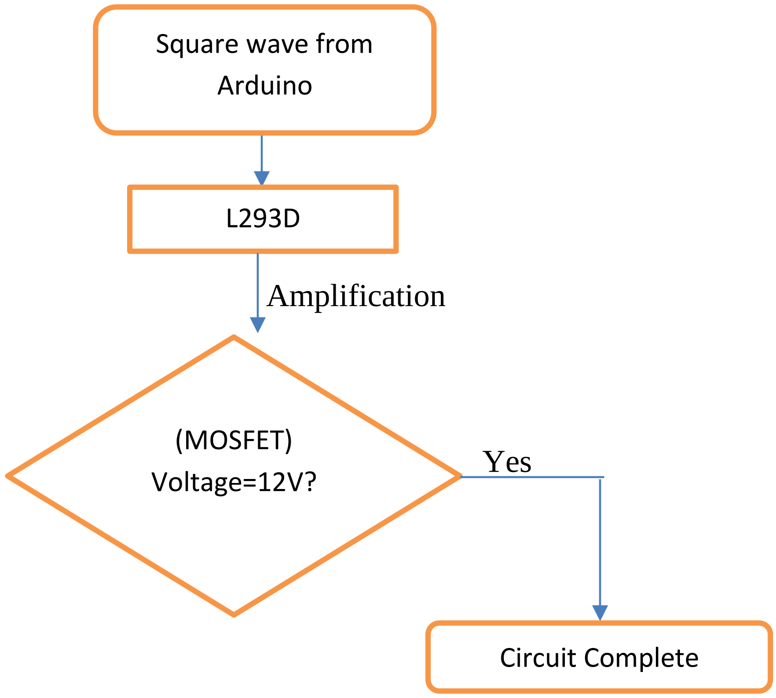

Figure 38 : Flowchart for working of Control System

5.2 Gesture Control System

This system works on the principle of capacitive coupling. As the controller (human hand in this case) comes near a metal sheet, due to the coupling between them, capacitance of the plate changes. The time of charging of a metal plate (capacitor) depends on its capacitance. Hence, we can find a relationship between the distance of the hand from the plate and the time of charging of the plate.

Three plates in three different planes are used and they are charged with 5V via 220K ohm resistances. Simultaneously, their time of charging is measured using an Arduino. Using the equation stated below, we can find out the co-ordinates of our hand in 3D.

$$\boxed{\textbf{Distance } \alpha \textbf{ square root (1/time)}}$$

This is the basic driving principle behind the working of this gesture control system.

Figure 39 below shows an illustration of the gesture control system.

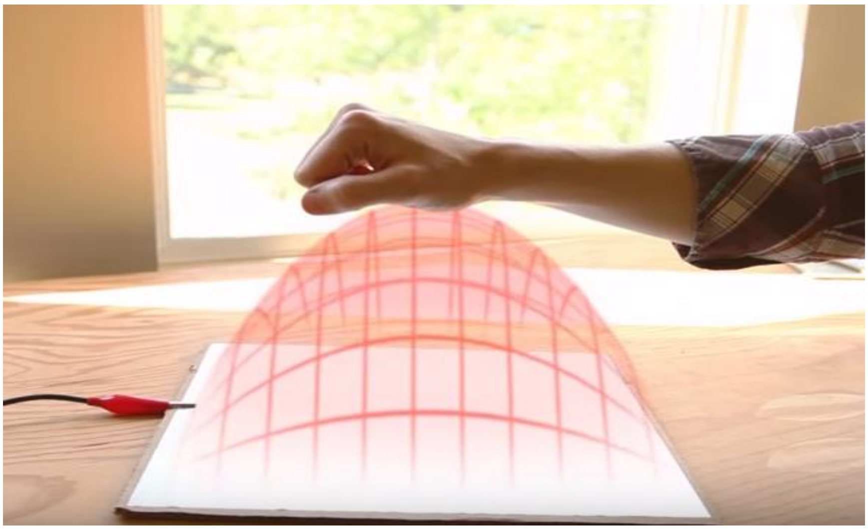

Figure 39 : Illustration for Gesture-Based Control

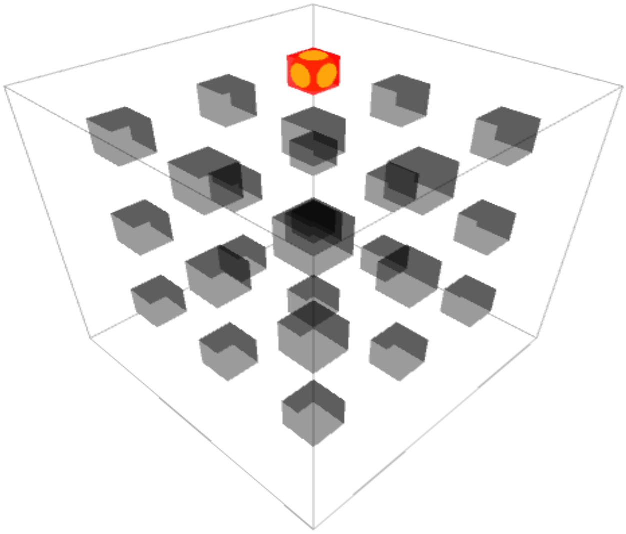

Figure 40 : Hand Position Display

Figure 40 above includes the software interface which shows the position of the hand (represented by the red block) by tracking it using the capacitance principle.

With a pre-made software in Processing, location of the hand can be seen in graphics and the same co-ordinates can be used to control different systems in 3D. Figure 41 below shows the actual working model along with the software interface for the Gesture Control System.

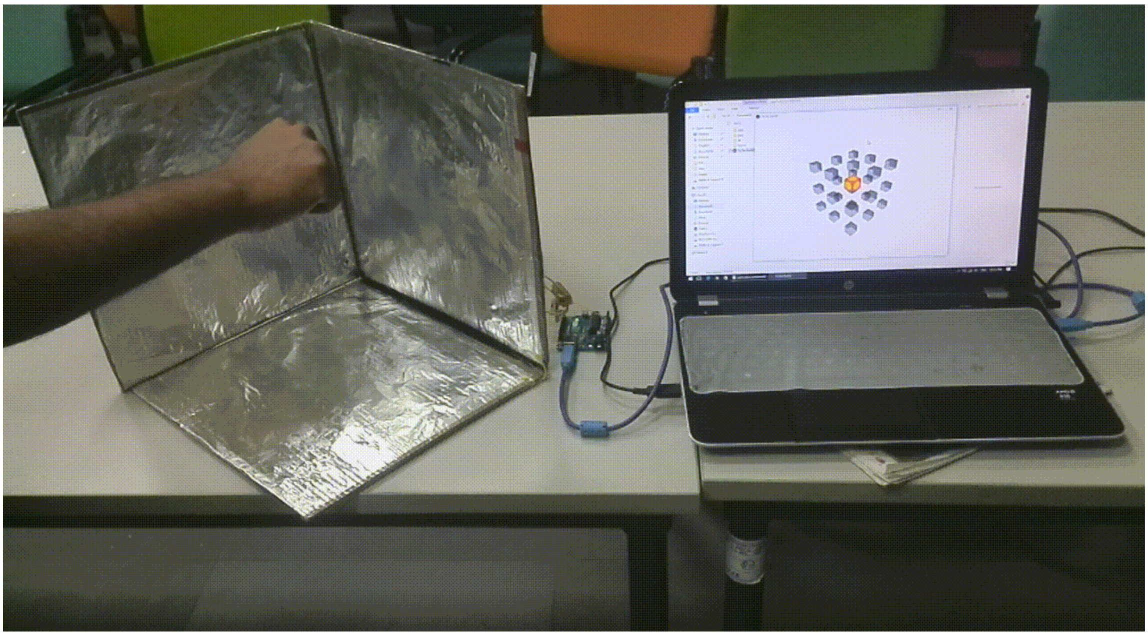

Figure 41 : Actual Gesture-based Control System Model

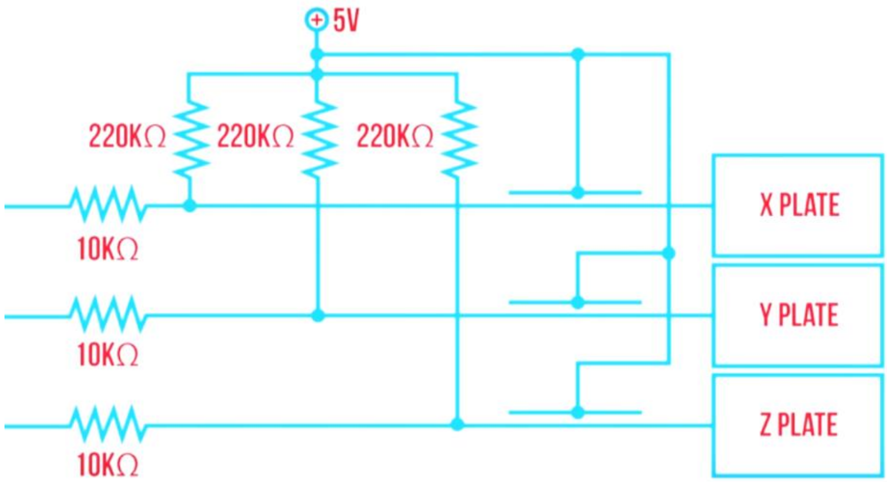

Figure 42 : Circuit Diagram for Gesture-based Control

Figure 42 above shows the circuit diagram for the Gesture Control System.

5.3 Universal Testing Machine

For linear displacement, a servo motor has been used and it is controlled using an Arduino and a stepper-motor controller. For calculating the load, a load-cell of capacity 50 N was used with a set of self-designed clamps for uniform force distribution. Figure 43 below shows the circuit diagram for the UTM showing load cell, power supply, stepper motor and Arduino.

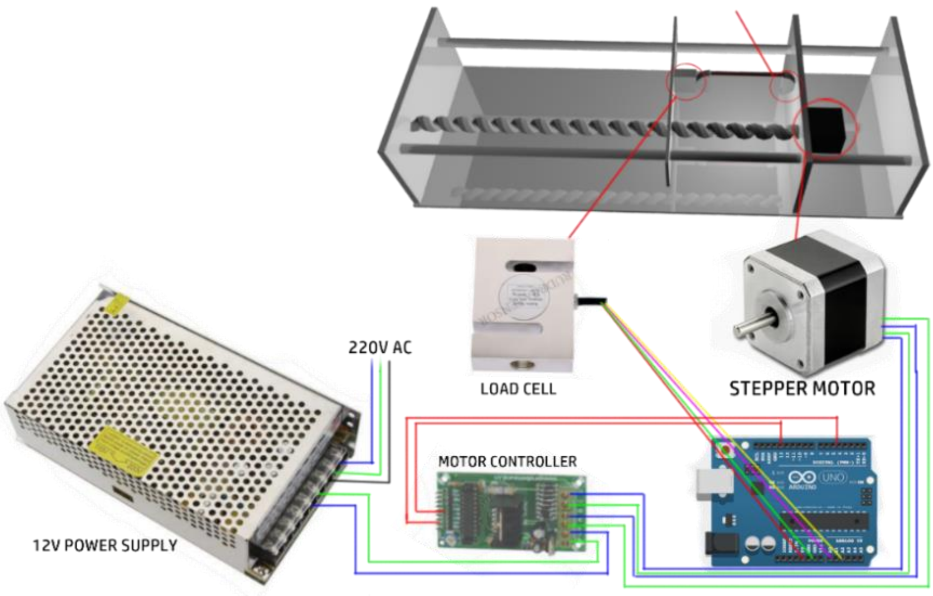

Figure 43 : Circuit Diagram for UTM

The circuit consist of a stepper motor, a motor controller, a 12V power supply to power motor controller, Arduino Uno, a Load cell and a Personal Computer (PC). Arduino works as a moderator unit and provides signal to motor controller as well as reads signal received from the load-cell. Arduino is to be connected to a PC in which the custom-made UTM software is installed, via USB.

For Controlling the UTM, a software with a customized GUI has been developed. It also provides different options for speed, loading and cycles etc. The interface has control options like RUN, PAUSE, STOP and EXPORT, and at same time it displays data in graphical format.

Figure 44 below shows the software interface used for controlling the different function of the UTM.

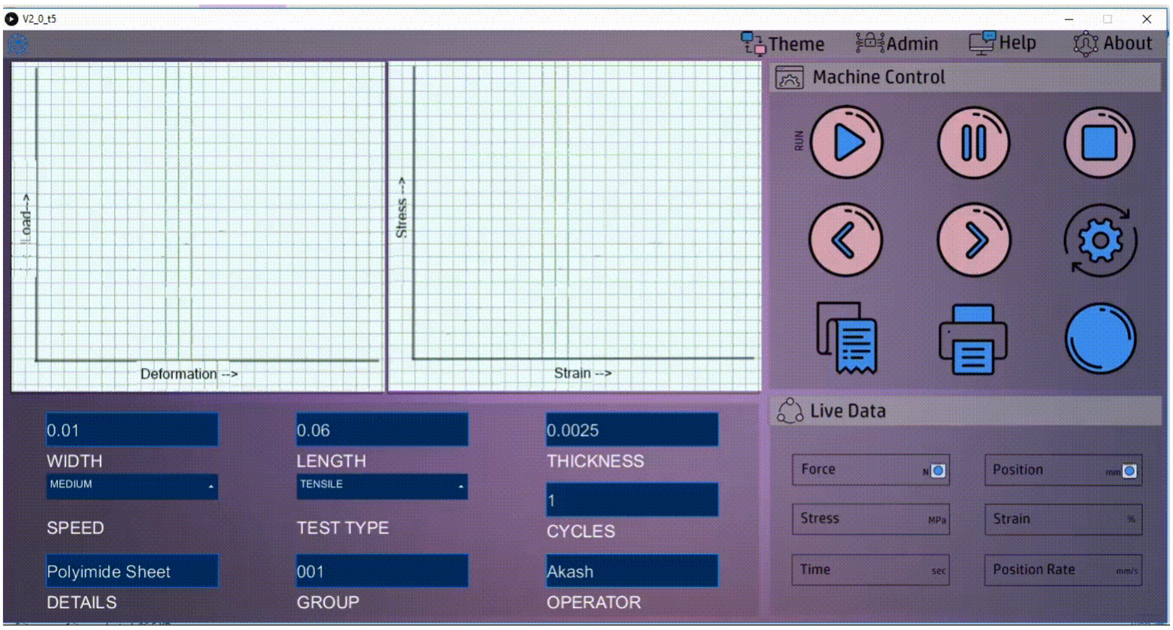

Figure 44 : Software Interface for UTM

Salient features of the Software:

- Easy to install & easy to use.
- Graphics user interface in vibrant colors and two theme options.
- Clear input options for all required details.
- Big and self-explaining icons for machine control.
- Live feedback and real-time data output in numeric as well as graphical format.
- The software enables user to take print-out of graphs as well as data in excel format.
- Password protection of Administrative features.
- Help is available in written and audio-visual form.
- The software is fully designed in an open source platform, PROCESSING.

Table 3 : Specifications of UTM Software

Software Specifications	
Platform Used	Processing 3.2.1
Compatible with	Windows XP or above
Hardware requirement	200 MB ROM, 1GB RAM

Table 3 above includes the specification requirements for the working of UTM Software.

CHAPTER 6 : PROGRAMMING LOGIC

6.1 Control System

In the designed control system, the Arduino provides a square wave of desired pulse-width and a 5 V amplitude. Pulse-width of wave can be changed for each of the positive and negative halves by making some slight modifications in the code.

```
void setup()
{
        Serial.begin(9600);
        pinMode(4, OUTPUT);
        pinMode(5, OUTPUT);
        pinMode(9, OUTPUT);
        pinMode(10, OUTPUT);
}
void loop()
{
        int volt_req = 7;        // ACTUATION VOLTAGE(0-12V)
        int cycle_time = 1000;   // HEATING-COOLING CYCLE TIME
        int volt_eq = volt_req*21;
        analogWrite(4, 0);
        analogWrite(5, volt_eq);
        analogWrite(9, 0);       // POSITIVE STROKE
        analogWrite(10,255);
        delay(cycle_time);
        analogWrite(9, 0);       // NEGATIVE STROKE
        analogWrite(10, 0);
        delay(cycle_time);
}
```

The Arduino code for actuation of the bimorph is the one included above. Program starts with defining Pin-mode for pins 4, 5, 9 and 10 as output pins and starts the loop function by initiating volt_req and cycle_time. Volt_req is then converted to equivalent voltage. The Arduino provides the desired voltage output through pin 4 and 5. The code will start providing 5 V square wave with desired the cycle time; 1000 milli-seconds in this case.

6.2 Gesture-Based Control System

As discussed earlier, time of charging is directly proportional to the distance of the hand from the metal plate. For calibration, the hand should be moved from the outermost position of diagonal to the innermost point, while pressing the left mouse button. The cube inside the remote is divided in 27 (3 x 3 x 3) smaller cubes of same size. After calibration, the outermost point is (3, 3, 3) and inner most point is (1, 1, 1).

For graphical interface, time of charging of all 3 plates is normalized and then plotted in a 3 x 3 x 3 matrix and displayed in 3D using an OpenGL library.

6.3 Universal Testing Machine

User interface for UTM is designed in processing and the following external libraries are being used -

- g4p_controls – For creating more than one window at any instance.
- controlP5 – For Dropdown List and Input Panel.
- java.util – For using Java Utilities.
- processing.pdf – For Pdf output of scree.
- vsync – For Data Synchronization between Arduino and Processing.
- processing.serial – For Serial Communication between Arduino and PC.

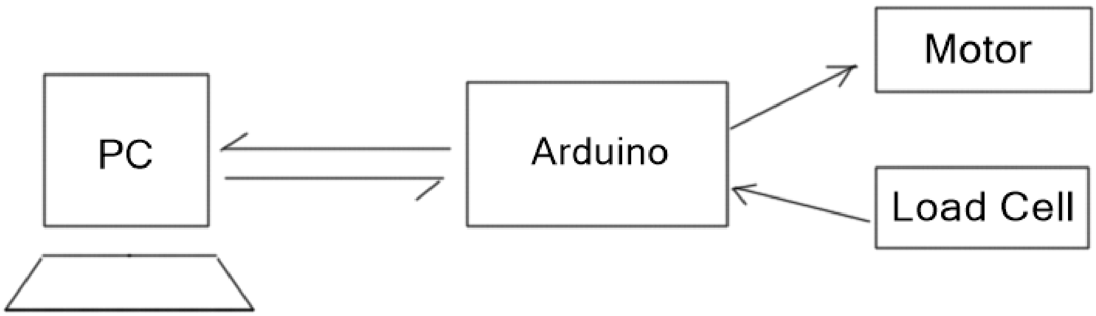

Figure 45 : Block Diagram for UTM

Figure 45 shows the Software Block Diagram for the working of the UTM.

Serial communication between Arduino and PC is stabilized at a rate of 19200 Bits per second. Different P-Image variables are formed and the images for background and icons are then loaded. Based on the mouse position and the machine status, different images are projected on the screen.

Data input is taken with the help of the controlP5 library and is stored in a character String format. Data of numeric values is converted into Float format using the float( ) function.

When the ‘Run’ button is pressed, the computer provides the direction data to the Arduino; based on type of test that is selected by the user and the stepper motor is started. With the motion of the moving plate, a force is exerted on the load-cell and the data values thus generated are read by the Arduino and transferred to the PC for data processing. The PC calculates the stress values as Load/Area and the strain values as Displacement/Length and this data is then plotted on a graph on the screen.

On pressing the ‘Pause’ button, the machine stops and the motor is locked in its position whereas on pressing the ‘Stop’ button, the machine stops but the motor is free to rotate.

When the ‘Print’ button is pressed, a screen shot of graphs is saved in Pdf format and on pressing the ‘Export’ button, data will be saved in an Excel sheet.

CHAPTER 7 : CONCLUSIONS AND FUTURE SCOPE

7.1 Conclusion

This project work is basically aimed at checking the suitability of in-house developed SMA Bimorphs of Cu-Al-Ni alloy in the field of Aerial Vehicles and the development of micro flappers for Micro Aerial Robots. Composite films of Cu-Al-Ni, of composition Cu 84.5%, Al 11% and Ni 4.5 % by weight; are developed by Physical Vapor Deposition on polyimide substrate. These composite films were found to have Two Way Shape Memory Effect at a transformation temperature of nearly 220-230° C. Due to their Two Way Shape Memory Effect and High Energy Density, these composite sheets are found to be suitable to be used as flappers for Aerial Robots.

To actuate the SMA Bimorph, Joule heating was used. For a continuous heating-cooling cycle, voltage in the form of a square wave form was provided. To generate a square wave of a higher frequency, a control system was developed as the Programmable Power Supply was not capable of providing the desired frequency. This self-developed system is monitored and controlled using an Arduino.

After the development of Bimorphs and the Control System, different experiments were performed on it for life-cycle analysis, frequency-displacement analysis and analysis of physical properties. To check the uniformity and thickness of deposition of the alloy on the substrate, experiments were performed using a 3D profilometer. The composition of the SMA was verified using an X-ray Diffraction machine. From the experiments for life-cycle analysis, it has been concluded that there is no loss in shape memory properties of bimorph, even after 1000 cycles.

The flapper of an aerial vehicle should be capable of supporting the body’s weight. For which these flappers should vibrate at a sufficient frequency. Some tests were performed on the bimorph and a frequency of 20 Hz, observable using LDS was achieved. The maximum frequency recorded in any well-known publication till date was 3 Hz. Along with this high frequency, a load carrying capacity of 150 mg was achieved and the maximum displacement achieved was 4.5 mm, which was verified experimentally using an LDS system.

For testing physical properties of SMA Bimorph and investigating their behavior with temperature change, a UTM machine was developed with integrated temperature control and a user-friendly Graphical User Interface. The UTM machine is capable of performing experiments for tensile, compressive and cyclic loading. The self-developed UTM can not only be used for analysis of Physical properties, but also to find and/or verify the phase transformation temperature of the SMA Bimorph.

For finding transformation temperature, a calorimeter is generally used but for this, the specimen must be in powdered form. As the specimen in this case is a Bimorph, this was not possible. Since Shape Memory Alloys change their physical properties with activation temperature, it is proposed that performing physical properties' analysis in controlled ambient temperature can provide information about the transformation temperature of SMA, and this technique is very useful for bimorphs.

7.2 Future Scope

By performing various tests and experiments, it can be concluded that SMA Bimorph can be a suitable option for flappers for MAVs. It is better than electric motors due to its simplistic design and high power density. But further development in this field is still required to use SMA in the aviation field.

Also, it could be said that by if the maximum displacement obtained, the maximum force generated and the maximum frequency attained; could all be achieved simultaneously i.e. at the same time, then it would be possible to attain flight. This, however, has to be combined with a much smaller chassis to be used for the MAV, so that the weight is reduced as much as possible.

7.3 Publications

- Design and Development of Micro-Aerial Robots using Cu-Al-Ni/Polyimide Composite
  (International Conference on Shape Memory and Super-Elastic Technologies)

REFERENCES

1) Ti-Ni-Cu-polyimide composite-film actuator and simulation tool - *Akira Ishida*

2) Ti-Ni-Cu shape-memory alloy thin film formed on polyimide substrate - *A. Ishida, M. Sato*

3) Shape memory behavior of Ti-Ni alloy films sputter-deposited on polyimide substrate - *Yoichi Kishi, Noriaki Ikenaga, Noriyuki Sakudo, Zenjiro Yajima*

4) Shape Memory Alloy and Elastomer Composite MEMS Actuators - *P.D. Fallon, A.P. Gerratt, B.P. Kierstead, R.D. White*

5) Substrates for Flexible Electronics: A Practical Investigation on the Electrical, Film Flexibility, Optical, Temperature, and Solvent Resistance Properties - *Valerio Zardetto, Thomas M. Brown, Andrea Reale, Aldo Di Carlo*

IMAGE SOURCES

Figure 1 :
http://ardupilot.org/copter/_images/3DR-quad-motors-top.jpg

Figure 2 :
http://www.actionmodelcentre.com/prodimages/dragonfly%20L.jpeg

Figure 3 :
http://image.slidesharecdn.com/sma-140508073622-phpapp01/95/shape- memory-alloys-principles-and-applications-7-638.jpg?cb=1405001111

Figure 4 :
https://en.wikipedia.org/wiki/File:SMAoneway.jpg

Figure 5 :
https://en.wikipedia.org/wiki/File:SMAtwoway.jpg

Figure 6 :
http://voitlab.com/courses/thermodynamics/images/1/1b/SMA_Comparison_to_other.png

Figure 7 :
Ti-Ni-Cu shape-memory alloy thin film formed on polyimide substrate - A. Ishida, M. Sato

Figure 39 :
http://makerflux.com/wp-content/uploads/2013/01/3D-tracking-interface-360x240.jpg